NAVAL POSTGRADUATE SCHOOL

MONTEREY, CALIFORNIA

THESIS

EXTREME WAVE STATISTICS WITHIN THE MOUTH OF THE COLUMBIA RIVER

by

Carter L. Johnston

December 2014

Thesis Advisor: Thomas H. C. Herbers
Co-Advisor: Jamie H. MacMahan

THIS PAGE INTENTIONALLY LEFT BLANK

REPORT DOCUMENTATION PAGE

Form Approved OMB No. 0704-0188

1. AGENCY USE ONLY *(Leave blank)*	2. REPORT DATE	3. REPORT TYPE AND DATES COVERED
	December 2014	Master's Thesis

4. TITLE AND SUBTITLE
EXTREME WAVE STATISTICS WITHIN THE MOUTH OF THE COLUMBIA RIVER

5. FUNDING NUMBERS

6. AUTHOR: Carter L. Johnston

7. PERFORMING ORGANIZATION NAME(S) AND ADDRESS(ES)
Naval Postgraduate School
Monterey, CA 93943-5000

8. PERFORMING ORGANIZATION REPORT NUMBER

9. SPONSORING /MONITORING AGENCY NAME(S) AND ADDRESS(ES)
N/A

10. SPONSORING/MONITORING AGENCY REPORT NUMBER

11. SUPPLEMENTARY NOTES: The views expressed in this thesis are those of the author and do not reflect the official policy or position of the Department of Defense or the U.S. Government. IRB Protocol number ____N/A____.

12a. DISTRIBUTION / AVAILABILITY STATEMENT
Approved for public release; distribution is unlimited

12b. DISTRIBUTION CODE

13. ABSTRACT (maximum 200 words)

Rogue waves have presented unpredictable, dire hazards to mariners since the dawn of seafaring. Even in benign seas, isolated rogue waves can severely endanger ships and crews, even accounting for their disappearance. Better understanding of rogue wave generation will enhance safety of maritime operations. This study examines surface height data from wave resolving drifters (WRDs) deployed in groups of 30–50 in the Mouth of the Columbia River (MCR) during the peak of ebb tide in May and June of 2013.

Over three separate collection days, effects of opposing currents and bathymetry on swell and wind waves were analyzed as WRDs headed to sea from the MCR. Wave significance was identified based on the local sea state within 1 km of the drifter location. Wave height histograms were calculated from regional wave ensembles and compared with the theoretical Rayleigh distribution of a narrow band, Gaussian wave field.

Generally, wave height data in the MCR follow Rayleigh distribution well. Areas over shallower bathymetry of the MCR Bar and predominant waves from the west create intense sea state amplification and rogue wave occurrence, and right-tail deviation from the Rayleigh pdf. Isolated extreme waves and trains of large waves were observed on the Bar.

14. SUBJECT TERMS RIVET II, Extreme Waves, Rogue Waves, Histogram, Nonlinear, WRD, Wave Buoys, Awesome, Amazing, Mouth of Columbia River, MCR, Bar.

15. NUMBER OF PAGES
79

16. PRICE CODE

17. SECURITY CLASSIFICATION OF REPORT	18. SECURITY CLASSIFICATION OF THIS PAGE	19. SECURITY CLASSIFICATION OF ABSTRACT	20. LIMITATION OF ABSTRACT
Unclassified	Unclassified	Unclassified	UU

NSN 7540-01-280-5500

Standard Form 298 (Rev. 2-89)
Prescribed by ANSI Std. 239-18

THIS PAGE INTENTIONALLY LEFT BLANK

Approved for public release; distribution is unlimited

EXTREME WAVE STATISTICS WITHIN THE MOUTH OF THE COLUMBIA RIVER

Carter L. Johnston
Lieutenant Commander, United States Navy
B.S., Jacksonville University, 2004

Submitted in partial fulfillment of the
requirements for the degree of

MASTER OF SCIENCE IN METEOROLOGY AND PHYSICAL OCEANOGRAPHY

from the

NAVAL POSTGRADUATE SCHOOL
December 2014

Author: Carter L. Johnston

Approved by: Thomas H. C. Herbers
Thesis Advisor

Jamie H. MacMahan
Co-Advisor

Peter C. Chu
Chair, Department of Oceanography

THIS PAGE INTENTIONALLY LEFT BLANK

ABSTRACT

Rogue waves have presented unpredictable, dire hazards to mariners since the dawn of seafaring. Even in benign seas, isolated rogue waves can severely endanger ships and crews, even accounting for their disappearance. Better understanding of rogue wave generation will enhance safety of maritime operations. This study examines surface height data from wave resolving drifters (WRDs) deployed in groups of 30–50 in the Mouth of the Columbia River (MCR) during the peak of ebb tide in May and June of 2013.

Over three separate collection days, effects of opposing currents and bathymetry on swell and wind waves were analyzed as WRDs headed to sea from the MCR. Wave significance was identified based on the local sea state within 1 km of the drifter location. Wave height histograms were calculated from regional wave ensembles and compared with the theoretical Rayleigh distribution of a narrow band, Gaussian wave field.

Generally, wave height data in the MCR follow Rayleigh distribution well. Areas over shallower bathymetry of the MCR Bar and predominant waves from the west create intense sea state amplification and rogue wave occurrence, and right-tail deviation from the Rayleigh pdf. Isolated extreme waves and trains of large waves were observed on the Bar.

THIS PAGE INTENTIONALLY LEFT BLANK

TABLE OF CONTENTS

THIS PAGE INTENTIONALLY LEFT BLANK

LIST OF FIGURES

THIS PAGE INTENTIONALLY LEFT BLANK

LIST OF ACRONYMS AND ABBREVIATIONS

APD	Average Wave Period (seconds)
ATMP	Air Temperature (degrees Celsius)
DPD	Dominant wave period (seconds)
ESA	European Space Agency
ERS	European Remote-Sensing
GPS	Global Positioning System
GST	Wind Gust (m/s)
H_s	Significant Wave Height
IMU	Inertial Motion Unit
LASH	Lighter Aboard Ship
MCR	Mouth of the Columbia River
MWD	Mean Wave Direction for DPD
PRES	Pressure (hPa)
WDIR	Wind Direction (degrees True)
WRD	Wave Resolving Drifter
WSPD	Wind Speed (m/s)
WTMP	Sea Surface Temperature (degrees Celsius)
WVHT	Significant wave height (meters)

THIS PAGE INTENTIONALLY LEFT BLANK

ACKNOWLEDGMENTS

My most sincere gratitude is given to Professor Tom Herbers for both his patience and guidance throughout the pursuit of my thesis work. I am fortunate that I was given the opportunity to work with Tom, a well-known expert in the field of the nearshore coastal environment. Because of his guidance, I was able to make the most of this challenging learning experience.

I spent countless hours spinning my wheels attempting to figure out MATLAB in analyzing countless wave data. Paul Jessen's MATLAB prowess helped get me back on pavement so that I could move forward with my analysis. He is a MATLAB genius. I would not have been able to create the thesis products that I did without Paul's generous help and dedication.

My gratitude is given to Jamie MacMahan, who agreed to be my co-advisor. Jamie also broadened my understanding of time series analysis and the nearshore environment.

To Steve McIntyre, Doug Pearman, and others who collected the data that was used in my thesis, I could not have done this thesis without their hard work.

Thanks go to my classmates. It has been my pleasure to know them; it will be my honor to continue serving in the fleet with them. Until we meet again, fair winds….

Finally, to my family, the love and support they have shown me has only been matched by their patience and understanding. Time and time again, they have enabled me to succeed. I owe them my most heartfelt gratitude.

THIS PAGE INTENTIONALLY LEFT BLANK

I. INTRODUCTION

A. HISTORY AND BACKGROUND

Rogues, freaks, extreme waves—these are names used to describe a force of nature so powerful and mysterious that it shares the same nautical folklore as mermaids and sea monsters. Ships and their crews crushed or swallowed in a single gulp, or simply never seen or heard from again: this is the stuff of legend. The scientific community has debated their very existence, and although their presence has not been confined to the open ocean, the occasional arrival of rogue waves near populated shores has often been mistaken for either tidal waves or tsunamis. The thorough, scientific study of massive waves is relatively new. Hardly a product of tall tales told by drunken fishermen, these waves do in fact, exist, and they are extremely relevant to our way of life. Our very own disciplined and reputable navy was not immune to the rogue wave's appearance or destruction, or confusion as to its very nature.

On August 29, 1916, the USS *Memphis* (CA 10) was anchored in relatively calm waters off the coast of Santo Domingo, Dominican Republic, when the crew spotted a massive wall of water approaching from the horizon. Although the wave took over 40 minutes to reach the ship, it was not nearly enough time to finish bringing all the necessary boilers up to steam for maneuvering to safety (Pararas-Carayannis 2007). The ship was carried forward to the shore and battered to a rocky death, and sat abandoned for years until finally salvaged for steel. Although the loss of the ship was attributed to what was then called a tsunami, the captain was found at fault for not preventing the catastrophe. While there is no record or evidence of seismic activity that would have likely caused a tsunami along the coast of Santo Domingo during that time, there were two hurricanes that passed within the vicinity of Santo Domingo in August, 1916, one of which passed within 250 miles of Santo Domingo's coast as a Category II hurricane on August 29 (Pararas-Carayannis 2007).

Another example of how the understanding of rogue waves is relevant to the U.S. Navy is given by a 34-meter (112-foot) rogue wave measured using triangulation

methods by the officers of USS *Ramapo* (AO 12) as they battled for their lives in a storm in the Northern Pacific while in transit to the Philippines on February 7, 1933. Only a combination of calm discipline and pure luck spared the ship and her crew to deliver the first credible record of rogue wave activity (Smith 2006).

The shear overwhelming destruction of rogue waves often leaves no trace of its victims behind, adding to the legendary status of their existence. Large ships are no exception to being lost with hardly a trace. It is now theorized that a great number of ships that were lost at sea with presumed causes such as crew negligence or inexperience, shoddy or incomplete maintenance, or other human error, were actually resultant from the ever elusive freak wave (Rosenthal 2006). Owing to both facts that large ships are not impervious to rogue waves, and that the mysterious loss of a ship cannot always be attributed to incompetence of the crew or maintenance personnel, the state-of-the-art MS *München* and crew were completely lost at sea on December 13, 1978 during a routine Atlantic crossing (Rosenthal 2006). The MS *München* was a German Lighter Aboard Ship (LASH) that displaced almost 45,000 tons, was 261 meters long, and 32 meters in beam. She carried a seasoned, expert crew of 28 on her 62nd voyage across the North Atlantic. Because of exceptional flotation capabilities of the LASH platform, *München* was considered by many to be practically unsinkable (Busch 2014). Nevertheless, after several distress calls, the MS *München* and crew were never seen again. Although nearly 80 vessels and 13 aircraft intensely searched the area of MS *München*'s last mayday transmission for 7 days, the largest trace of it ever found was a single lifeboat. The best clue as to her fate rests in the sheared retaining pins that once secured the boat nearly 20 meters above the *München*'s waterline: they had been sheared by an extreme force horizontal force (BBC 2002).

Despite the rapid strides forward in advanced science and oceanic exploration, the mysteries of the deep still hold all but near the surface in uninterrupted concealment. It has only been within the last 75 years that humanity has begun to understand the true nature of these legends. Only within the last 30 years has there been a verified scientific affirmation through instrumental measurement of an extreme wave.

Beyond installing instruments (such as pressure sensors or downward pointing optical sensors) from a fixed platform, or measuring wave heights from satellite, a third method of studying rogue waves is through the use of surface-following buoys equipped with GPS and/or onboard accelerometers (Herbers 2012). In coastal areas with strong currents and ship traffic, moored buoys or fixed platforms are difficult to maintain, and these single point measurements may not capture the wave amplification on shoals. In contrast, drifting buoys can be deployed with relative ease in almost any environment, and the use of numerous drifter buoys increases the chances of detecting rogue waves both through increase in sensor numbers and from transit through areas thought to contain rogue waves (Herbers 2012).

The coastal environment of the Mouth of the Columbia River is ideal for the study of rogue waves. As the fast flowing waters of the Columbia River rush out to sea, energetic incoming swells steepen on the opposing currents and are focused by refraction over the large ebb-tidal shoal surrounding the mouth of the river, causing the well known spectacular waves feared by mariners. Because of these ideal conditions for rogue wave development, the area acts as a natural laboratory for study.

With over 200 super cargo ships lost at sea between 1981 and 2000, and an average of two vessels per day lost at sea worldwide (Rosenthal 2008), understanding, and one day predicting the occurrence of rogue waves serves to increase the safety and efficiency of seaborne operations. Predicting and thus avoiding potential rogue wave events could have a tremendous positive impact on the safety and efficiency of maritime operations. Any research leading to understanding rogue wave occurrence can only serve to benefit naval operations at sea. While rogue waves most often occur in the open ocean, they also occur close in to shore, an area that the navy is ever-increasingly finding itself operating in during this 21st century, including missions such as humanitarian relief and disaster assistance.

B. OBSERVED ROGUE WAVES

On January 1, 1995, the first scientific measurement of a rogue wave was recorded on the Draupner platform (58.1° N, 2.28° E) in the North Sea, in 70 meters of

water and off the coast of Norway (Haver 2000). Using a downward aimed laser sensor, the extreme wave measurement of over 25 meters (shown in Figure 1) was correlated with minor damage that was sustained on the platform by the same wave.

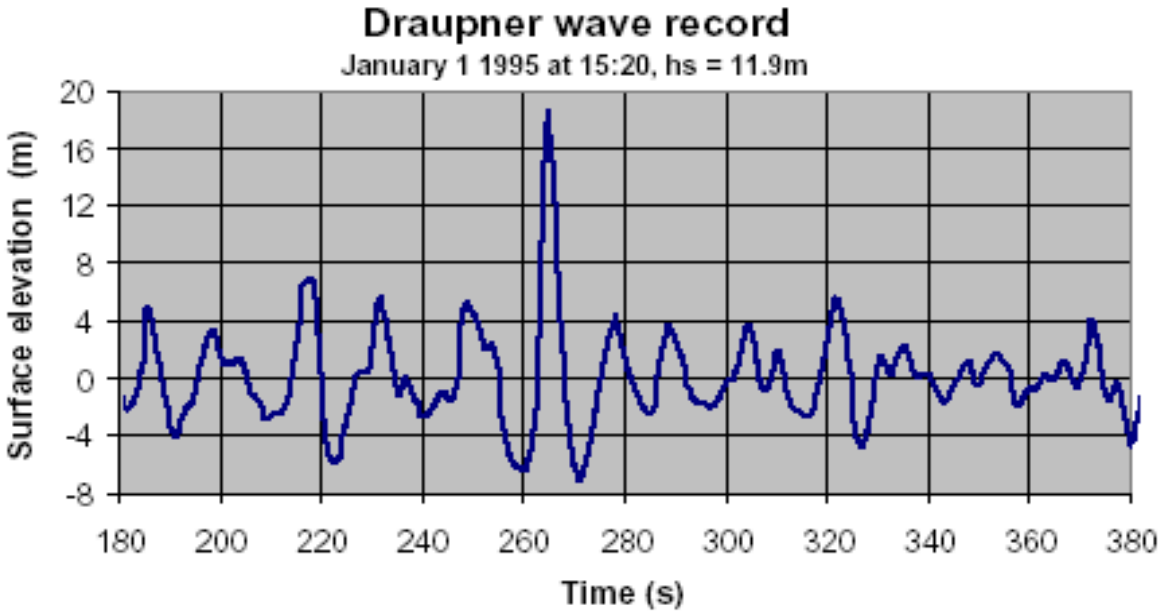

Figure 1. Draupner wave record from the January 1, 1995 rogue wave measuring over 25 meters in height (from Paul H. Taylor, University of Oxford).

Since the measurement of Draupner's New Year wave, research has been ongoing. Generally, the occurrence of rogue waves was found to fit within the theoretical Rayleigh distribution of a narrow-band, Gaussian sea state (Figure 2), and as such, are the normal expected occasional occurrence of extreme wave events over a long period of time (Thornton and Guza 1983). Much research has been conducted to test that assumption, and recent research has pointed to mechanisms for rogue wave generation that may lead to more frequent occurrence under certain conditions.

In December of 2000, W. Rosenthal and a team of German scientists, supported by the European Space Agency (ESA), combed through 3 weeks of wave data acquired from ESA's European Remote-Sensing (ERS) radar satellites from twin spacecraft ERS-1 and ERS-2 (Rosenthal 2008). Through the use of these advanced satellite-based radar,

Rosenthal's research team poured over more than 30,000 images in 10km by 5km resolution. This study, known as the MaxWave Project, identified more than 10 individual rogue waves, measuring more than 25 meters in height, around the globe (Rosenthal 2008). These 10 rogue waves came both as a surprise and realization that massive waves are much more common than expected by standard Rayleigh theory (Rosenthal 2008).

C. ROGUE WAVE THEORY

Rogue waves are defined through their relationship with significant wave height, H_s. This is a value that is usually defined in one of two ways: 4 multiplied by the value of the variance of the wave spectrum, raised to 0.5 power ($4m_0^{1/2}$) (Forristall 2000), or the average of the top 1/3 highest ($H^*_{1/3}$) of all waves in a given sea state (Stansell 2004). Generally, it is accepted that rogue waves can be caused by wave refraction along bottom topography. Also contributing to the formation of rogues is the collision of waves against an opposing current, causing a wave or wave train to stack up, thus creating a wave that exceeds the threshold for what is considered a rogue, in our study, H>2H_s.

Among the few theories for rogue wave generation, one of the most commonly accepted is the statistical expectation of outliers in a random process. That is to say that when a large number of waves are observed in a given sea state, a certain percentage of them will fall into the rogue wave category. This theory uses the Rayleigh wave height probability density function (pdf) that is illustrated in Figure 2 and is expressed by:

$$p(H) = \frac{2H}{Hrms^2} \exp\left[-\left(\frac{H}{Hrms} \right)^2 \right]$$

where the root-mean-square wave height $Hrms = \sqrt{\frac{1}{N}\sum_{m=1}^{N} H_m^2}$ and is approximately equal to $\frac{Hs}{\sqrt{2}}$.

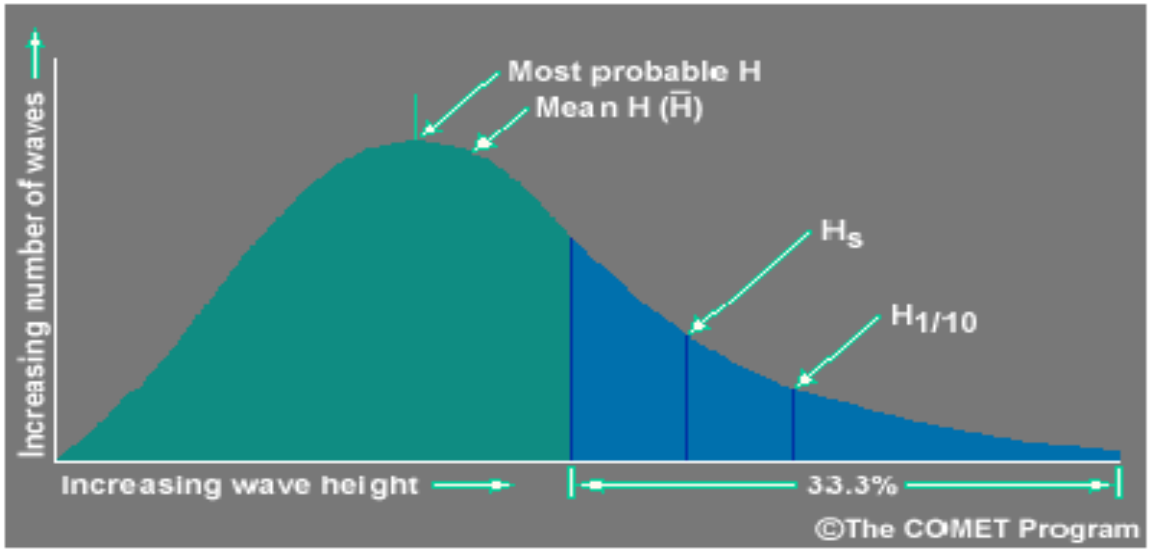

Figure 2. Rayleigh distribution for waves (from: University Corporation for Atmospheric Research, COMET)

Strictly speaking, according to Rayleigh statistics, rogue waves should occur in any given sea state at a rate of 1 per 3,333 waves, or about 0.03 percent of all waves: this has been observed by several studies, including a 6-year study covering 50,359 hours of measurements from a gas-drilling platform offshore from Mossel Bay, South Africa, alongside the Agulhas Current (Lui and MacHutchon 2006) and is depicted on the far right tail of the Rayleigh pdf in Figure 2.

The superposition of wave fields, or the method of constructive interference, is yet another theory behind rogue wave formation (Figure 3), and is the product of combining several waves together.

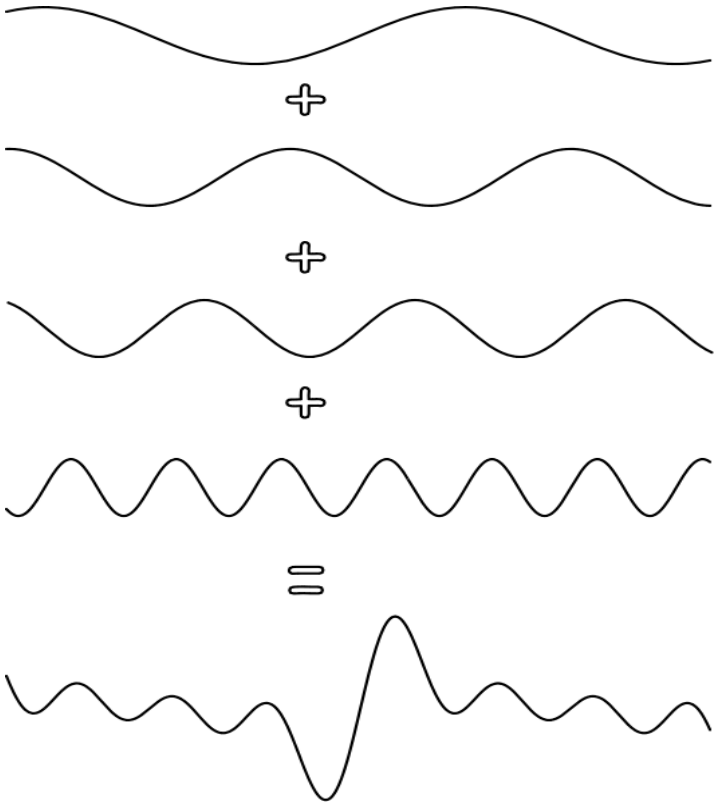

Figure 3. Superposition of waves at the top result in the product on the bottom. (from John D. Norton, University of Pittsburgh)

In the vast expanse of our world's oceans, there are an infinite number of wave trains travelling at different speeds and different directions, and that on occasion, enough of them will cross paths in one brief, constructive, rogue wave moment. Because these are not single waves but the joining of many intersecting, travelling waves, they appear seemingly out of nowhere and will disappear just as quickly.

Non-linear, or energy stealing waves, is another theory for rogue wave generation. Through non-linear processes governed by the Nonlinear Schrödinger equation $\left(i\,\partial_t \psi = -\frac{1}{2}\partial_x^2 \psi + \kappa |\psi|^2 \psi \right)$, and shown by Dysthe (1996), waves can actually sap energy from other nearby waves. One of the simplest known solutions to the Nonlinear Schrödinger equation is known as the "breather wave." It starts with a simple modulated wave that "breathes" upward at the expense of its neighbors and is a good example of the process of rogue wave generation that is behind this theory (Figure 4). However, the

near-ideal conditions required for the breather wave solution make it an unlikely rogue wave candidate outside of a controlled laboratory environment.

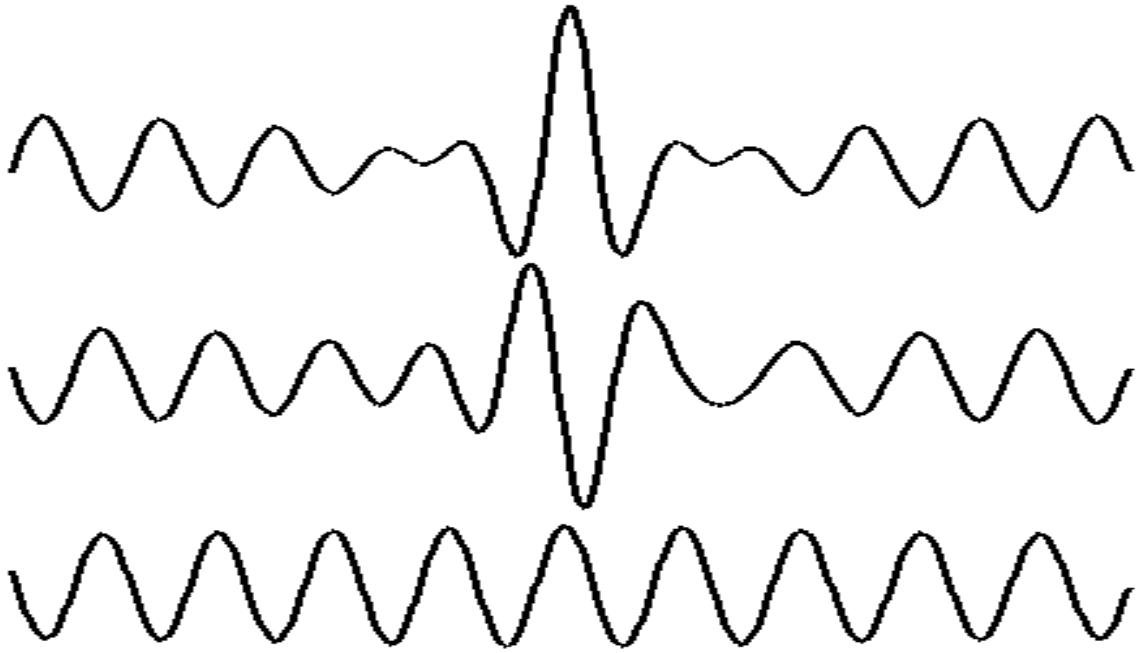

Figure 4. The nonlinearly generated “breather” wave in 3 stages: the first stage at the bottom, followed by the next 2 stages of growth at the expense of neighboring waves. (from Dysthe, University of Oslo).

In some areas of the world, such as in the vicinity of the Kuroshio Current off Japan’s coast, or the Agulhas Current off the coast of South Africa, large-scale ocean currents flow in opposition to prevalent surface winds. In these scenarios, ocean wave energy is focused (Figure 5) by variable or opposing currents and the wave profiles are shortened and heightened due to the wave-current interaction (Rosenthal 2008). Commonly, ships rounding the Cape of Good Hope heading west would ride the Agulhas current to save time. During the Suez Canal closure from the Israel-Arab War (1967-1975), a spike in maritime mishaps was noted in the vicinity of the Agulhas, as more ships were faced with taking this route and deciding to ride the current, sometimes coming face-to-face with the wave-stacking effect of wave energy focusing.

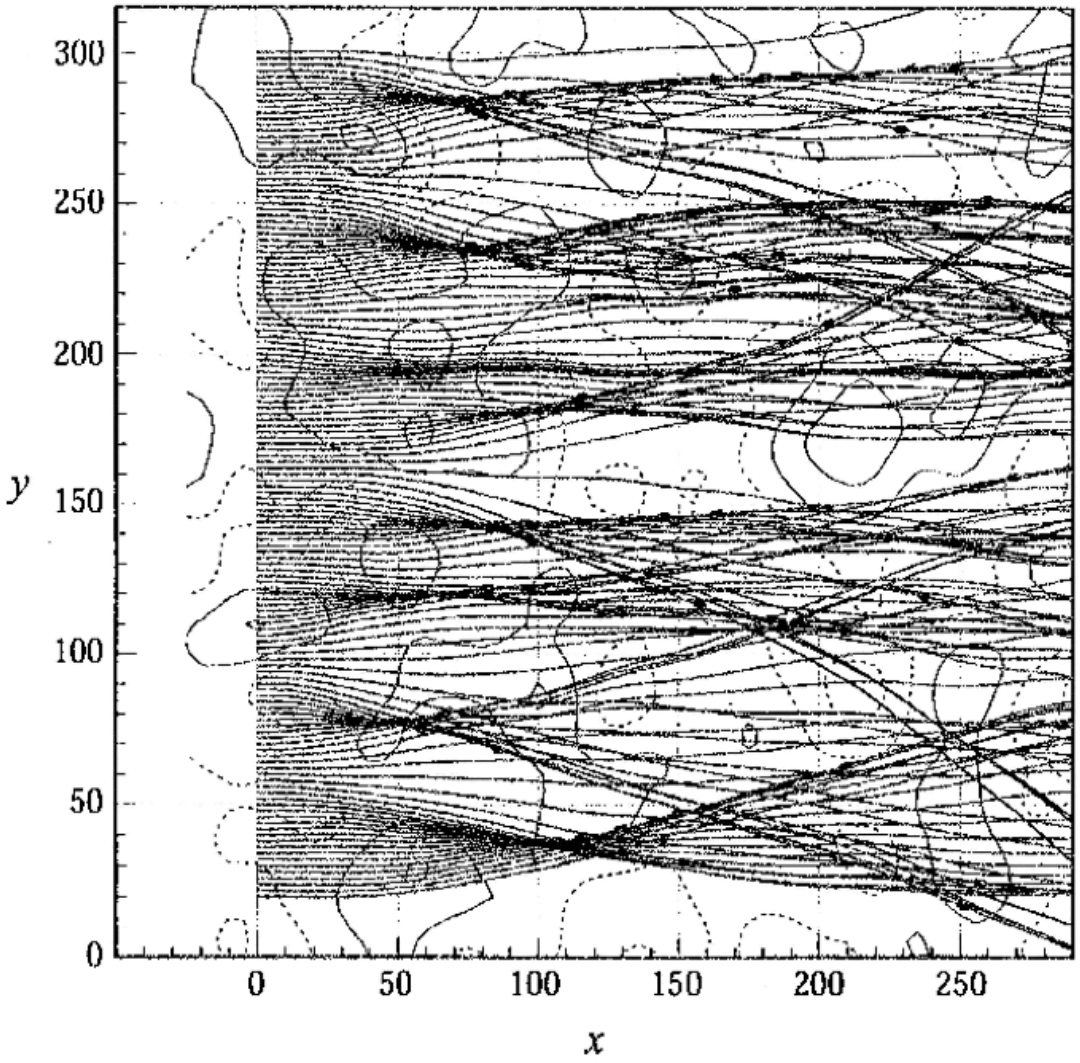

Figure 5. Depiction of current focusing caused by wind-current interaction. (from White and Fornburg 1998)

In the case of opposing currents, the current field induces a refractive caustic along the principal current axis. Caustic focusing causes an increase of wave height to its maximum, and this rapid wave amplification can trigger nonlinear instabilities that form even larger rogue waves (Janssen and Herbers 2009). In this scenario, the largest waves are found upstream of the caustic area (around x/Lo=25 in Figure 6).

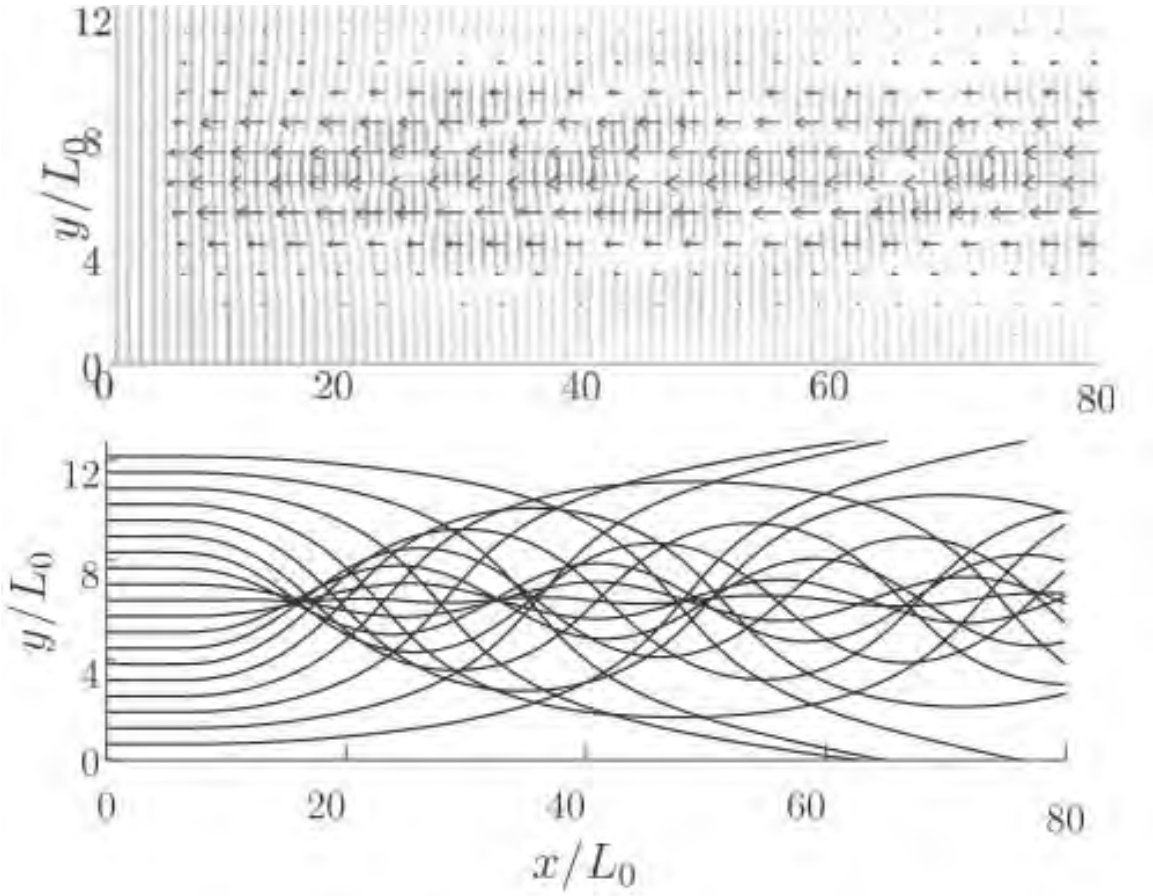

Figure 6. Transformation of 0.1-Hz swell incident from left on opposing current. Upper panel: wave crests (shading indicates the height) and current vectors. Lower panel: ray trajectories (from: Janssen and Herbers 2009).

Alternatively, focusing can result, especially in coastal regions, from underwater topographic features with effects similar to those shown in Figure 6. In both instances, ray trajectory focusing creates a convergence of wave energy; the sudden increase in wave height triggers the nonlinear instability that produces rogue waves (Janssen and Herbers 2009).

D. SCOPE

This thesis will determine the characteristic location of rogue waves in the Mouth of the Columbia River (MCR) where ocean swell are strongly affected by interactions

with strong ebb tidal currents and the ebb tidal shoal system. Observed wave height statistics will be compared with the Rayleigh distribution for a linear narrowband wave field. Previous studies of wave statistics in coastal environments have relied mainly on a very limited number of fixed sensors in a less dynamic environment than the Mouth of the Columbia River. In the ONR-funded RIVET II experiment, a large number of drifting wave buoys equipped with GPS and Inertial Motion Unit (IMU) or accelerometer sensors were deployed in the Mouth of the Columbia River, providing a unique opportunity to study the wave variability in this region. Better understanding of how and where rogue waves form in this complex coastal environment will increase the safety margin in both naval and civil maritime operations nearshore.

THIS PAGE INTENTIONALLY LEFT BLANK

II. FIELD EXPERIMENT AND DATA

In May and June of 2013, scientists from the Oceanography Department of the Naval Postgraduate School and Theiss Research, with funding from the Office of Naval Research, participated in the multi-organizational RIVET II research experiment in the Mouth of the Columbia River and vicinity. Over a 3-week period, focus was directed to the study of abnormally large waves, and possibly rogue-waves, in the nearshore river-outlet environment of the Columbia River Mouth.

A. FIELD SITE AND EXPERIMENT

Its mouth located along Oregon coast's famed "Graveyard of the Pacific," the Columbia River boasts a raging length of over 1,200 miles fueled from a watershed spanning seven U.S. states and the Canadian province of British Columbia at its origin. The combination of strong, tidal currents and a rapid river outflow produce maximum ebb currents of four to seven knots. Owing to these strong currents, the Columbia River lacks the characteristic delta that often slows and tames a river's currents as it empties into the sea. Instead, strong, focused, fire-hose-like currents have deposited a large sandbar that shallows the waters outside of the mouth as its waters rush by to collide with the oncoming assault from the sea. For these reasons, the Mouth of the Columbia River (MCR) is considered to be an ideal location for the study of abnormally large waves, and holds a great potential for rogue wave generation. Since 1792, over 2,000 vessels have sunk in the immediate vicinity of the MCR due to extreme coastal wave conditions.

In a cooperative effort between University of Washington, University of California, University of Miami, Theiss Research, and the Naval Postgraduate School, a field experiment was conducted in this area between late May and early June of 2013. Because of the seasonal variations of this region, such as the winter storms characteristic of the area, and the springtime increase of water outflow from snowmelt, the selected period of late May through early June is the ideal time frame to observe strong wave-current interaction while wave conditions have moderated after the winter storms to facilitate safe vessel operations.

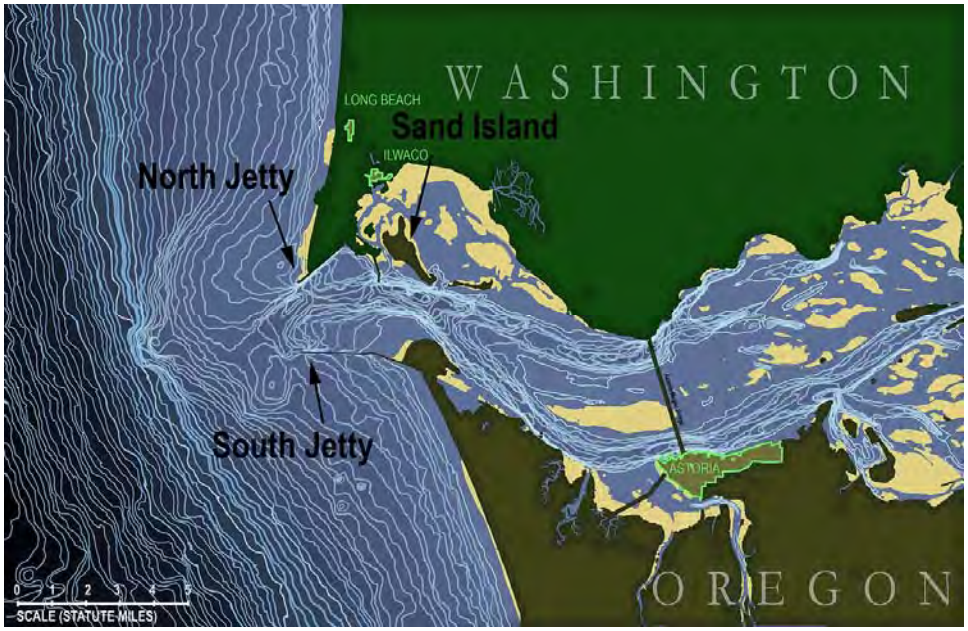

Figure 7. Bathymetry of Mouth of Columbia River area with depiction of North and South Jetty. Isobaths at five-foot intervals, 15-310 feet. Sandbars in yellow. (from K. D. Schroeder, en.wikipedia.org)

In order to capture possible rogue wave data, sensors would have to be stationed in areas that are believed to be conducive to producing rogue waves. Working from the wave-stacking theory that rogue waves can likely be generated by waves opposing strong currents, the ideal time for observing rogue waves is when ebb tides retreat back to sea with the river current strengthening it. This condition allows the maximum current from the river to meet the opposing waves from the sea. Because of the extreme conditions of this area, it would be very difficult and expensive to establish fixed sensors in the immediate area of interest, and could not be considered reliable due to the likelihood of being damaged or washed away by these strong, relentless currents.

Figure 8. Shipwrecks at the Mouth of the Columbia from 1829–2002. (from Map Bureau and Columbia River Maritime Museum)

Because of the strong opposing currents and dangerous environment described above, it was determined that drifter buoys would be the best platform for the task: drifters are free from any seafloor mooring requirement, and the associated cost savings allow the deployment of more sensors within a relatively short time with the freedom of deploying and retrieving within specific time periods of interest. Another benefit of using drifter buoys was the relatively quick turnaround time for collected data and the interchangeability of faulty buoys. A challenge of using drifter buoys instead of moored buoys was the additional complication of collecting data in a Lagrangian fashion instead of the stationary Eulerian method. Instead of being anchored in a specific area, the baseline or sea state for the sensor data was constantly changing with the movement and migration of the drifter. There were many challenges associated with accurately collecting motion and position data that are further discussed later.

B. EQUIPMENT AND DEPLOYMENT

Three basic variants of the Wave Resolving Drifter-buoy (WRD) were used in this study, each housed in a sturdy acrylic shell and equipped with GPS data loggers that measure geographic position and horizontal orbital wave velocity. Each WRD also houses 3-axes accelerometers used to measure wave motion.

The first variant of WRD has a 1Hz LocoSys GT-31 GPS data logger that records *u* and *v* Doppler velocity data and positional data, and has an X6-2 accelerometer housed in a waterproof Otterbox that is tethered beneath the drifter (McIntyre 2013 and Pearman et al. 2014). The second variant houses the same GPS unit found in WRD-A, but also includes a more sophisticated, Yei Technologies TSS-DL Inertial Motion Unit (IMU) accelerometer package (Portell 2013). Both WRD-A and WRD-B are equipped with Merlin 1/3N MX radiofrequency and Garmin DC-40 GPS transmitters for real-time line-of-sight tracking. The third variant, WRD-J is equipped with a 5Hz GPS data logger, an IMU accelerometer, and an Iridium transmitter for over-the-horizon real-time tracking.

A large number of drifters were deployed from the RV *Point Sur* during maximum ebb tide flow on three occasions. On each of the three days, the RV *Point Sur* maneuvered upstream of "The Bar" at the MCR and under full power, maintained a relatively stationary position against the current while the drifter buoys were deployed in groups of 3, each at 10-second intervals, while maintaining a one-minute interval between each group.

1. May 27, 2013, Deployment

At approximately 12:15 UTC, 27 drifter buoys (12 WRD-A, 9 WRD-B, and 6 WRD-J) were deployed at the beginning of ebb tide. Observed ebb currents were about 5 knots at the start of the deployment, increasing to 7 knots when all buoys were deployed. Winds were at 26 knots decreasing towards 15 knots and blowing in from the South. Significant wave height was 1.5 to 2 meters with a period of 6.67 seconds.

Waves travelling from the south-southwest throughout the day, combined with a southerly wind, caused the drifter buoys to head predominantly northward once clear of the strong river outflow during the ebb tide (Figure 9).

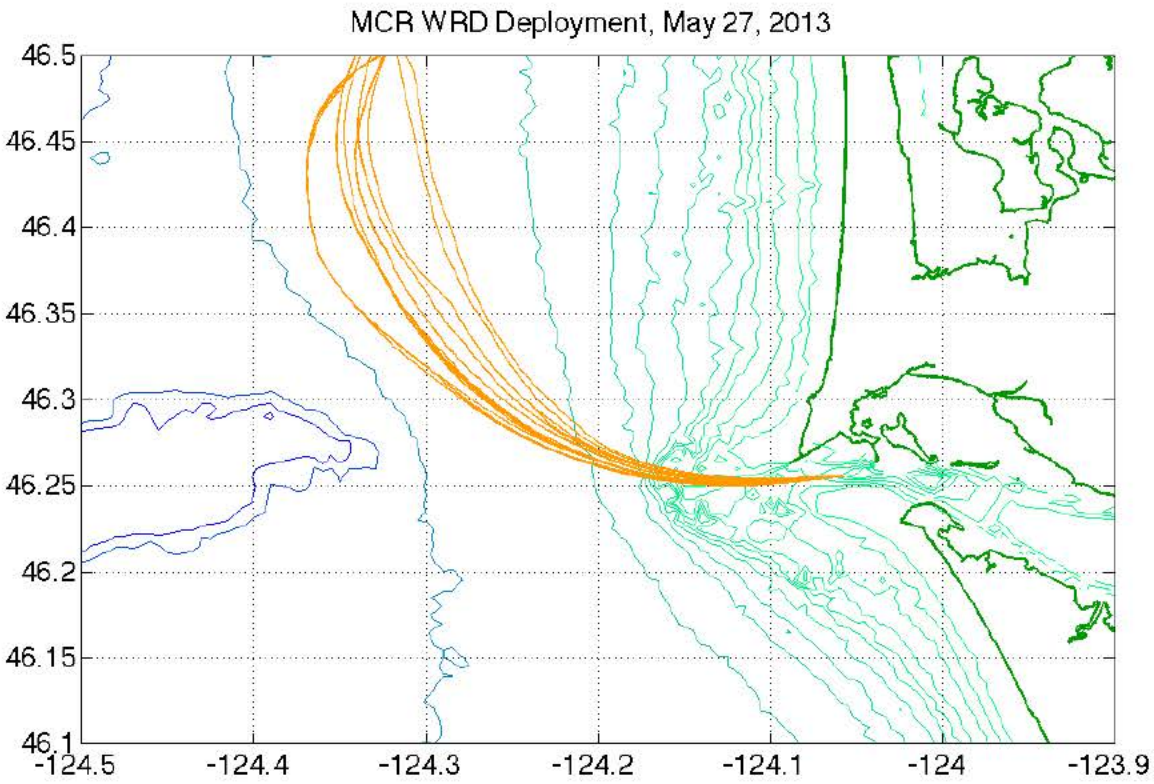

Figure 9. Day 1 Wave Resolving Drifter deployment. From left to right, depth contours in meters are: 200, 150, 100 (-124.5 to -124.3 Longitude), 50, 35, 30, 25, 22, 20, 18, 15, 12, 9.

2. May 29, 2013, Deployment

At 15:30 UTC, 44 drifter buoys (24 WRD-A, 11 WRD-B, and 9 WRD-J) were deployed, again at ebb tide. This time, the winds were a calmer, 12 knots, now blowing from the north-northwest. Currents were at 4.5 knots. Significant wave height averaged about 1.5 meters with an 8 to 9-second average wave period.

The drifter buoys maintained a westward course until well clear of "the Bar," then drifted northward and eventually doubled back towards the coast (Figure 10).

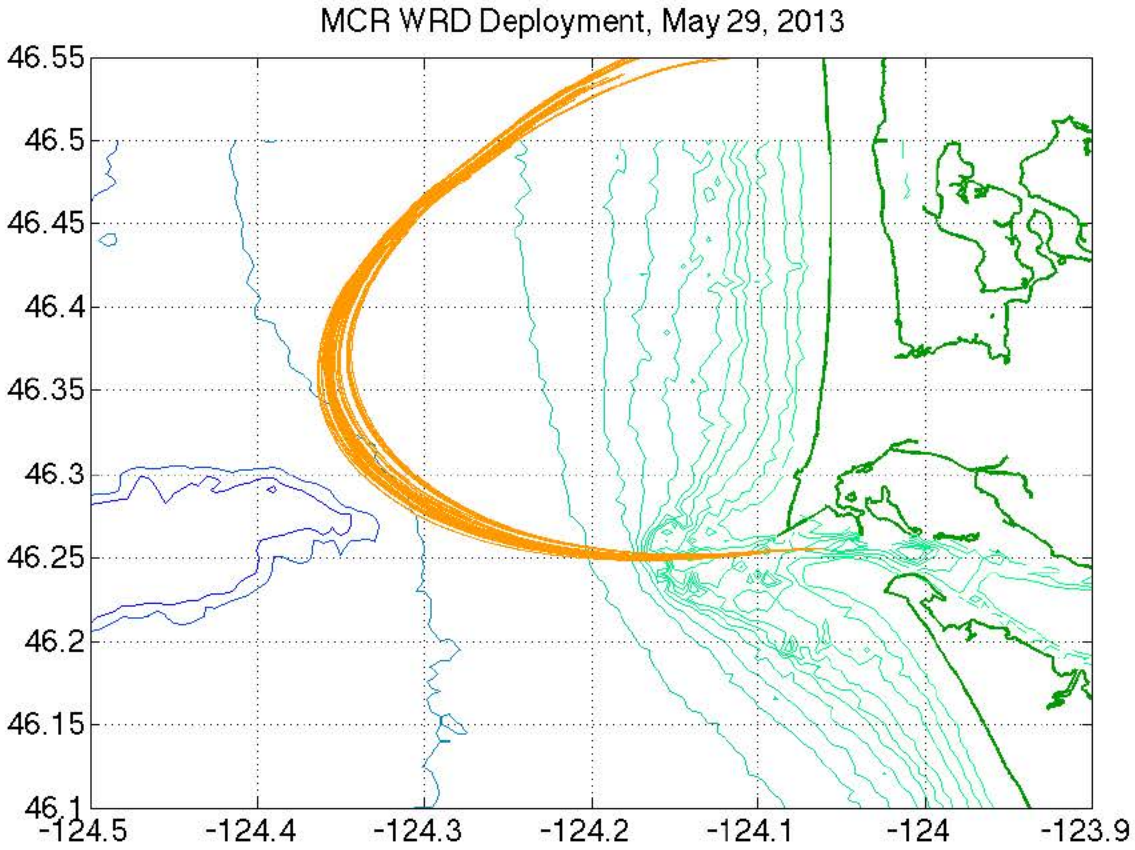

Figure 10. Day 2 Wave Resolving Drifter deployment. From left to right, depth contours in meters are: 200, 150, 100 (-124.5 to -124.3 Longitude), 50, 35, 30, 25, 22, 20, 18, 15, 12, 9.

3. June 8, 2013, Deployment

On June 8, 2013, at 12:00 UTC, 30 drifter buoys (13 WRD-A, 9 WRD-B, and 8 WRD-J) were deployed in a 5-knot ebb tide current. Winds were from the north-northwest at 10–15 knots; significant wave height was up to 2.5 meters with an average period of 16.67 seconds and an 8-second swell.

Waves travelled predominately from the west at 258° (True); predominant winds were from the north-northwest. Favorable winds and seas allowed the drifters a relatively straight course towards the west over the Bar and out to sea (Figure 11).

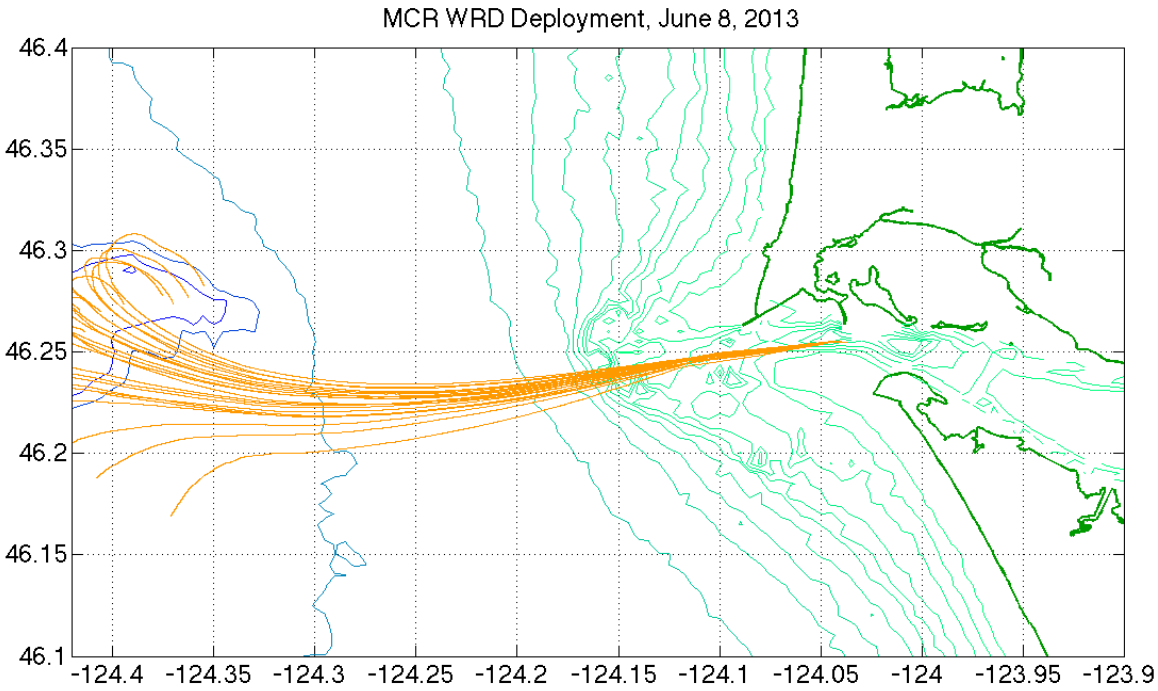

Figure 11. Day 3 Wave Resolving Drifter deployment. From left to right, depth contours in meters are: 200, 150, 100 (-124.5 to -124.3 Longitude), 50, 35, 30, 25, 22, 20, 18, 15, 12, 9.

C. DATA STREAMS COLLECTED

Both WRD-A and WRD-B used 1 Hz LocoSys GT-31 GPS data loggers, while the newer WRD-J used an upgraded 5Hz GPS data logger. Both GPS units are used to provide measurements for horizontal wave orbital velocities, UTM *x* and *y* positions, GPS output time, and latitude and longitude positions. Latitude and longitude are used for geographical referencing, while horizontal orbital velocities are later processed into wave height and velocity data. The LocoSys GT-31 GPS receiver accuracy is highest in the swell frequency band (~0.05-0.15 Hz) and is used in conjunction with the accelerometer package, which has its strengths in the higher frequency range (Pearman 2014). Thus, the strengths and weaknesses of both sensor types compliment each other.

Model WRD-A uses the Gulf Coast Data Concepts, LLC X6-2 accelerometer suspended below the WRD by steel chain ballast weight, while the upgraded WRD-B uses the Yei Technologies TSS-DL IMU located inside the buoy. At a 10 Hz sampling rate, the X6-2 accelerometer outputs acceleration measurements of +/- 2g (1g= -9.81m/s^2)

along 3 axes. The TSS-DL IMU also has an accelerometer that outputs g-force measurements, but also adds angular motion measurements from its gyroscope, and magnetic magnitude and direction measurements in gauss units from its magnetometer. All output measurements are along 3 axes, sampled at a 10 Hz rate, and run through a Kalman filter (Portell 2013). In this study, only the vertical component of acceleration that was available from all platforms is used.

III. DATA ANALYSIS

A. RAW DATA TO SEA SURFACE HEIGHT

In order to estimate wave surface height from the raw velocity and acceleration data from the WRD GPS and accelerometer, respectively, spectral data from both onboard instruments was independently calculated through Fourier transforming the time series in segments of 8,192 data points (about 13.5 minutes) with 50% overlap. Fourier transformed wave data was then filtered to allow a range of 0.06–0.20 Hz to include the dominant swell and wind waves. Surface height amplitudes were estimated from the acceleration Fourier amplitudes by dividing them with the transfer function ω^2, where ω is the frequency of the wave. For the GPS velocity data, the component in the dominant wave direction was used which (for directionally narrow wave fields) has a transfer function to surface height, gk/ω , that is independent of the wave direction. The wave number k is given by the dispersion relation $\omega^2 = gk\tanh kH$, where H is the water depth. This transfer function was applied to the Fourier amplitudes of the velocity record to obtain surface height amplitudes. Transformed surface height Fourier amplitudes, obtained independently from the accelerometer and velocity data are then inverse-Fourier transformed to yield estimated surface wave height time series. In all but the first and last of the overlapping segments of inverse-Fourier transformed data, only the middle 50% of the 13.5-minute segments were kept to avoid window ringing effects of the boxcar window. Although Figure 12 shows good agreement between the GPS and accelerometer height data, accelerometer measurements are noisy at low swell frequencies; therefore the GPS data was favored for the bulk of the data analysis.

B. ZERO DOWN CROSSING ANALYSIS

In order to statistically analyze wave heights, it is necessary to break up the estimated surface height record into individual waves. A commonly used analysis approach, applied in this thesis, defines a wave as the profile between two successive zero down-crossings (Figure 12). The wave period is the interval between the two down

crossings and the corresponding wave height is the difference between the maximum and minimum surface height within each wave.

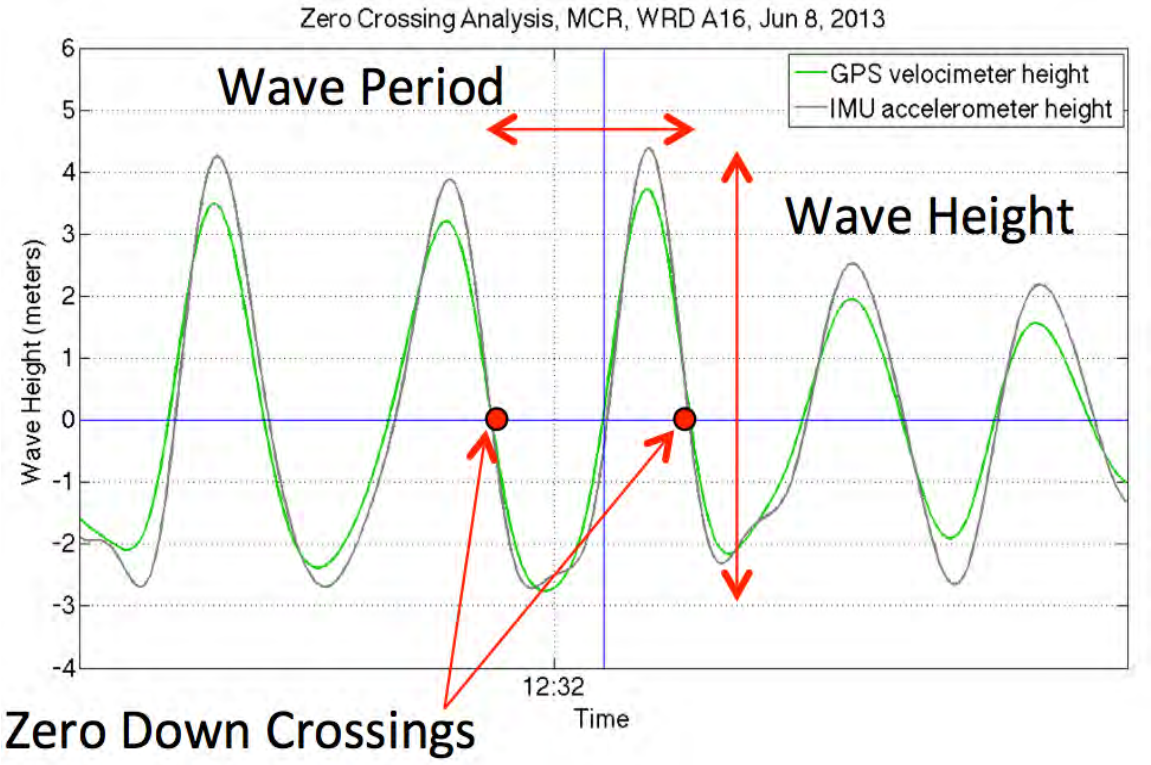

Figure 12. Estimated wave height data is analyzed through the zero down-crossing method.

C. WAVE ENSEMBLES

In order to determine the characteristic of a wave and assess whether it is common, extreme, or rogue, a sea state must be calculated. Sea state is the overall condition of the surrounding seas (wave heights) and is here defined as the root-mean-square wave height (H_{rms}) in a region surrounding the wave that is being evaluated. After a data base of individual surface wave heights has been established for all drifters, rogue waves are identified based on the ratio of the wave height H of each individual wave and the H_{rms} of all waves recorded within a 1 km radius. The 1 km radius was chosen to be large enough so that each ensemble includes a sufficiently large number of waves for a reliable estimate of H_{rms}, while still small enough that the sea state within the ensemble

region can be treated as approximately homogeneous. The number of waves per ensemble varied between 1,500 and 30,000. Based on the ratio H/H_{rms}, "extreme waves" were identified as those that exceed the threshold $H/H_{rms} > 2$ and "rogue waves" as those that exceed the threshold $H/H_{rms} > 2\sqrt{2}$ (equivalent to the commonly used criterion $H/H_s > 2$). This analysis requires a sea state calculation for each individual wave, determined by the surrounding waves within a given radius of distance. To put the value of modern computing into the correct perspective: for June 8 alone, a sea state has to be evaluated for over 60,000 waves! Although computationally demanding, this method gives us the most accurate depiction of sea state for any given wave, and is our preferred method for deciding how each individual wave compares to the peers around it. Through this analysis, we are able to determine whether a wave is "normal" (and boring), or exceptional, possibly rogue (and exciting and interesting).

While the size of the ensembles used for extreme and rogue wave detection was adequate for estimating H_{rms}, larger ensembles are needed to evaluate histograms of wave height. Therefore a second method of local sea state calculation is introduced here, based on comparing all waves within a certain longitudinal window. Due to complications resulting from a moving, Lagrangian timeframe, and moving drifters that travel at different speeds, we found it better to calculate local sea state based solely on longitudinal distance and separated into ensembles (Figure 13). Latitudinal distance was not considered to be a factor in our study because while close in to shore (our area of most intense interest), the WRDs all stay well within a few hundred meters of latitudinal position. Instead of calculating a sea state for over 60,000 waves on June 8, this method calculates local sea state based on all waves within each longitudinal window and is our preferred method for providing a reasonable, large amount of waves for histogram analysis.

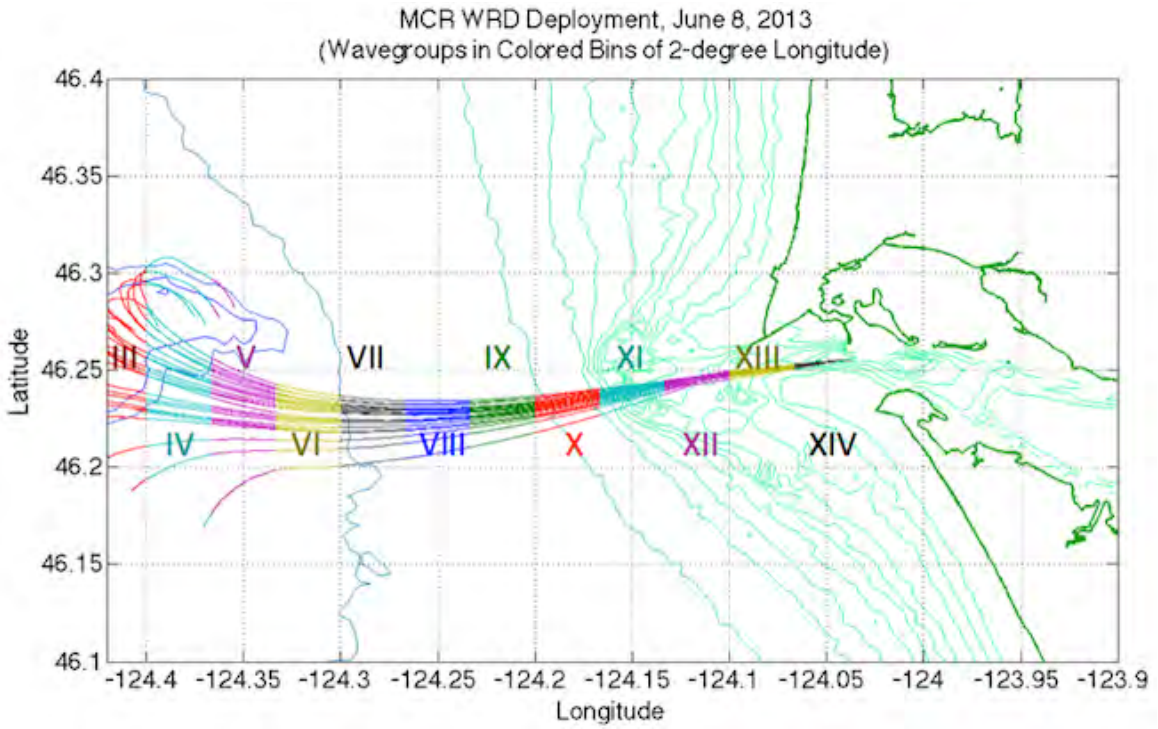

Figure 13. Wave height ensembles used to estimate histograms. Each colored region shows the portion of the drifter tracks within a 2-minute longitude interval that constitutes one ensemble.

On May 27, the data buoys travelled out past the MCR Bar, out to sea, and then turned north. By the time the drifters spread beyond our preferred distance from one another, or their turn north became less than optimal, our timeframe of interest was achieved. To prevent the mostly latitudinal direction of travel from affecting the sea state calculations, that data was eliminated. A similar issue was addressed for the May 29 data, in which the buoys crossed the bar, drifted out to sea, and then doubled back towards the coast. In the May 29 case, we eliminated the data once the drifters were out to sea and before they began to double back. In this way, any undesirable effects from spreading or latitudinal travel were negated by snipping off the data that fell outside our window of interest. We found that distance windows of 2 minutes longitude were the most effective in providing enough waves to have meaningful statistics, whereas longer distance ensembles tended to yield significant sea state variations within an ensemble that violates the assumption that all waves within the ensemble were observed in the same sea state.

D. HISTOGRAMS

Histograms were used in the statistical analysis of the wave data and were created for each longitudinal ensemble of sea surface data. Waves from each ensemble were separated into 50 histogram bins along the *x*-axis and determined by wave height, with bin height determined by the number of waves in each bin (*y*-axis). In order to ensure comparability between histograms from ensembles with different total wave count and varying sea state, both the *x* and *y*-axes were normalized. The *y*-axis bin height was normalized by dividing the number of occurrences by the total number of waves, multiplied by the bin width; the *x*-axis wave height values were normalized by H_{rms}. The total area under the resulting normalized histograms equals 1, allowing a direct comparison with the theoretical Rayleigh pdf (Figure 14).

The main purpose of this analysis is to test the hypothesis that the Rayleigh probability density function underestimates the occurrence of rogue waves under the conditions presented by the MCR environment. Even with nearly 250,000 recorded waves over three separate days, the formation of true rogue waves is still such a low-probability occurrence that a suitably accurate direct representation of their frequency requires significantly more time and waves. Because of the relationship between significant wave height and H_{rms}, it is useful to analyze rogue wave occurrence by proxy using the $2H_{rms}$ threshold discussed earlier. In analyzing the data with this requirement, we are able to show the actual occurrence of both types of wave compared to the theoretical Rayleigh pdf (Figure 14) and determine whether the expected occurrence is greater or less than what was observed at the MCR.

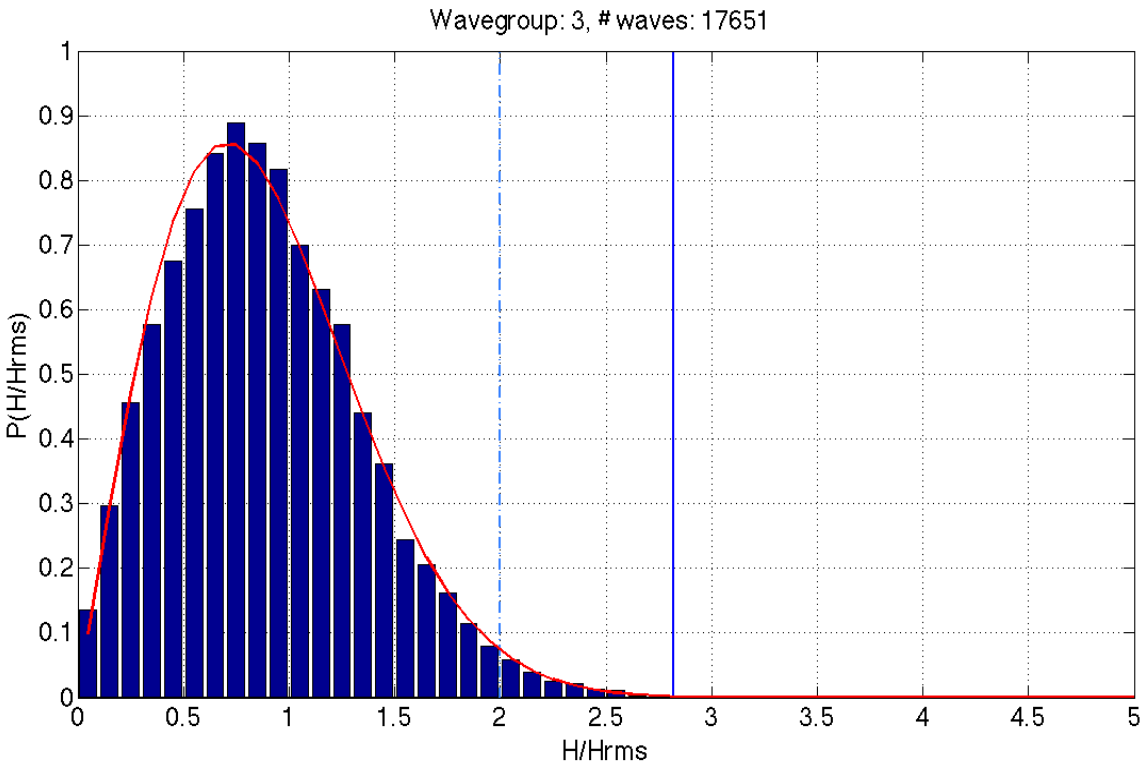

Figure 14. Example histogram created with 2-minute longitudinal ensemble from June 8th data from the Mouth of Columbia River, with theoretical Rayleigh pdf superimposed in red, a 2*Hrms* wave threshold depicted by vertical-dashed blue line, and $2H_s \approx 2.828$*Hrms* rogue wave threshold depicted with vertical blue line.

IV. OBSERVATIONS

The three days that observations were collected during ebb tide were quite different in wave direction, average wave period, swell, and wind speed and direction (see Appendices). May 27 was characterized by 15–26 knot winds from the south and a predominant wave direction from the south-southwest at 1.5 to 2 meters H_s with a 6.67-second period. On May 29, the winds were lighter, and from the north-northwest. The sea state was also calmer than on May 27, averaging around 1.5 meters H_s with an 8- to 9-second average wave period travelling from the west-southwest. On June 8, wind was from the northwest at 10–15 knots. Waves were dominated by a 16.67-second average wave period and an 8-second period swell from the west. The sea state was higher on June 8 than the previous two days with an H_s of up to 2.5 meters. All H_s values given are from the Clatsop Spit Waverider buoy data from Appendix A. These distinctly different wave conditions produce rather different extreme and rogue wave statistics as discussed below. The three case studies are discussed in chronological order.

A. MAY 27, 2013

More than 102,000 waves were collected on May 27 as the WRDs made their way over the Bar and out to sea, eventually turning north with the prevailing surface current. Because my primary interest was in the waves on and near the Bar and not those waves observed as the drifters headed north, I set a northern latitude limit of 46.3° N. Of the 102,202 waves recorded, a total of 20,126 waves were recorded in this area of interest. Of these waves, 453 (2.251%) exceeded the $2H_{rms}$ threshold for extreme waves, 40 (0.199%) of which were rogue waves ($>2.828H_{rms}$). Although the offshore wave conditions were rather benign on this day, with an average wave height of 0.85 meters, the maximum-recorded wave was 5.07 meters.

Because our area of interest was in the direct vicinity of the Bar, and our regional ensemble bins divided waves into groups by 2-minute longitude, the upper limit in latitude was determined to be an efficient way to eliminate influences on sea state calculations from the northern-drifting paths.

The first analysis was to calculate sea state for all the waves in the area of interest by comparison with all surrounding waves within a 1-kilometer radius from each of the 20,126 waves. From this sea state calculation, waves were plotted by type: regular wave ($<2H_{rms}$) marked by red dot and extreme wave ($>2H_{rms}$) marked by blue dot. Those extreme waves that met the traditional definition of rogue ($2H_s$, or ~$2.828H_{rms}$) are circled in black (see Figure 15).

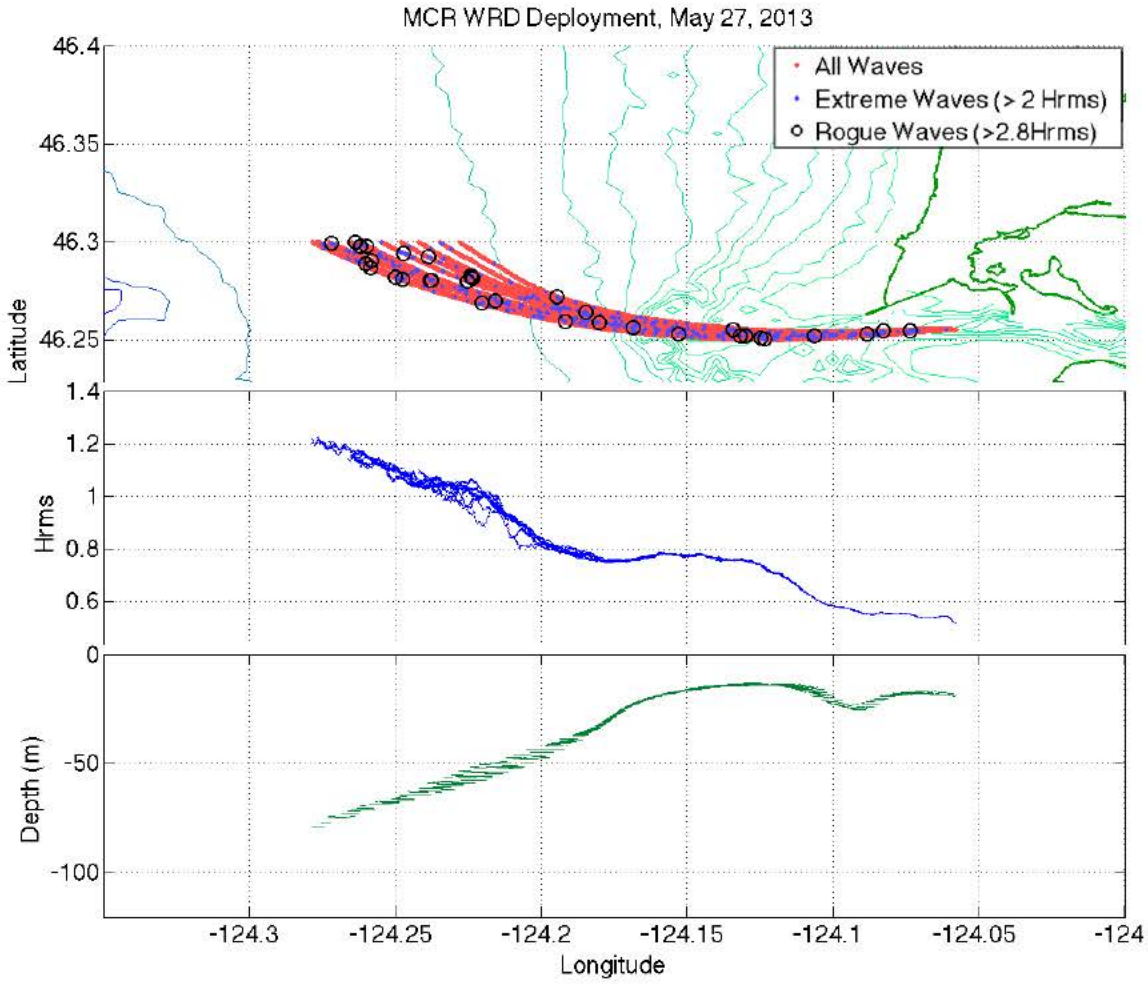

Figure 15. Top Panel: Wave heights of individual waves observed along the drifter tracks. From left to right, depth contours in meters are: 200, 150, 100, 50, 35, 30, 25, 22, 20, 18, 15, 12, 9. Middle panel: *Hrms* along each drifter track vs. longitude. Bottom panel: water depth along each drifter track vs. longitude.

Upon initial inspection, there does not appear to be any pattern to the occurrence of extreme waves: they seem to be dispersed randomly throughout the drift tracks, but with a distinct concentration in the area of the Columbia River Bar (Figure 16). The significance of the concentration of rogues in this area as compared to the seemingly high occurrence of rogues in deeper water near the western edge of the area of interest is more evident when considering the short amount of time spent in the vicinity of the Bar as they followed the ebb tide and river currents out to sea, whereas the drifters spend more time in deeper water and thus there is a larger density of observations.

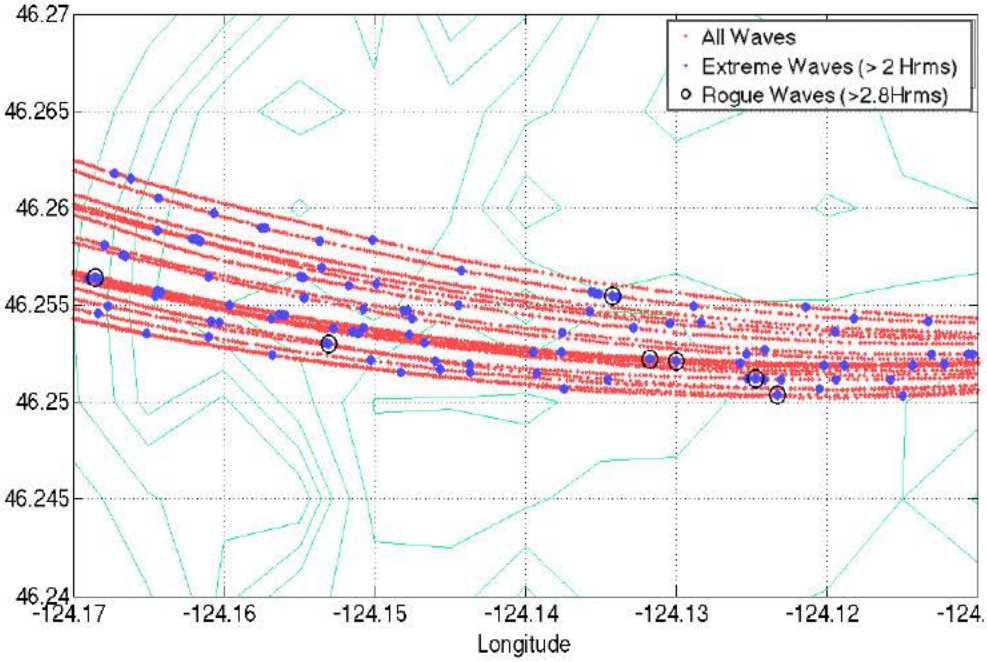

Figure 16. Blow up of the wave observations of Figure 15 for the Columbia River Bar area. Depth contours are from bottom left in meters: 30, 25, 22, 20, 18, 15, 9.

H_{rms} continued to trend upward as the WRDs drifted out to sea, with a slight enhancement over the Bar (see Figure 15).

Before dividing waves into ensembles, individual time series were investigated for validation and general observation. A few characteristic examples of rogue waves are shown in Figure 17. While the time series on the top panel of Figure 17 shows a more

distinct and isolated wave than the bottom panel, both these waves were included to illustrate that extreme and rogue waves on this day appear as isolated events, and not a succession of events.

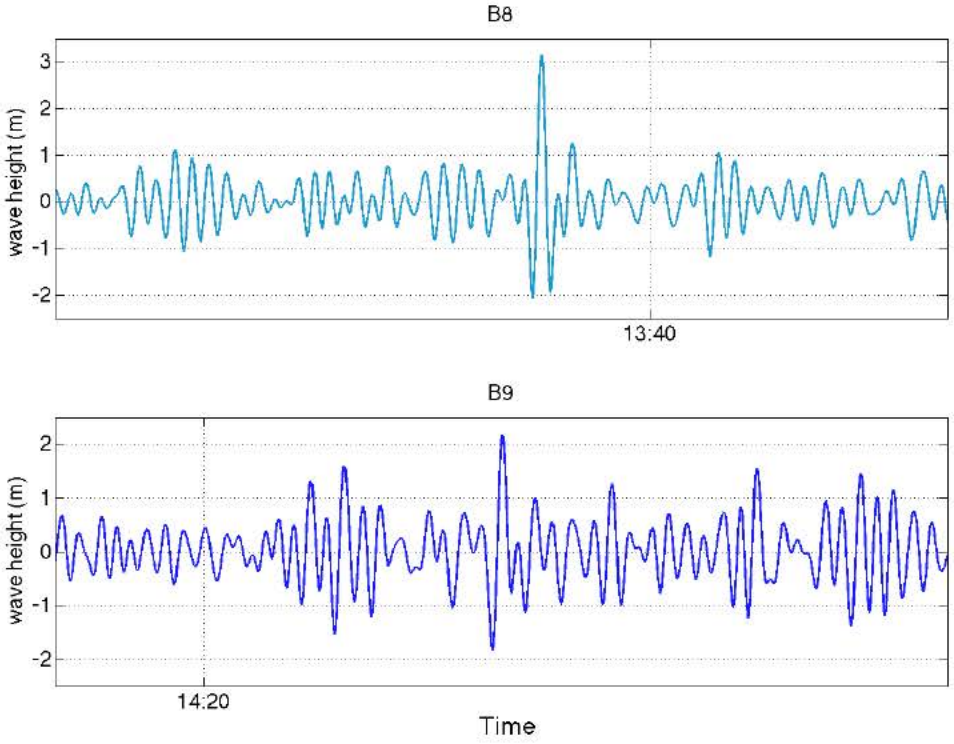

Figure 17. Both panels: 6-minute time series showing extreme wave events on May 27, 2013. Top panel: drifter B8. Bottom panel: drifter B9.

When looking at a rogue wave event experienced by drifter A22 during its transit over the bar, it experiences the same singularity and shape as shown by a similar event on the bottom panel of Figure 17. Figure 18 further illustrates that this isolated wave dwarfs all waves within its vicinity as measured by other nearby drifters making their transit over the bar. This is characteristic of what is expected when recording extreme wave events.

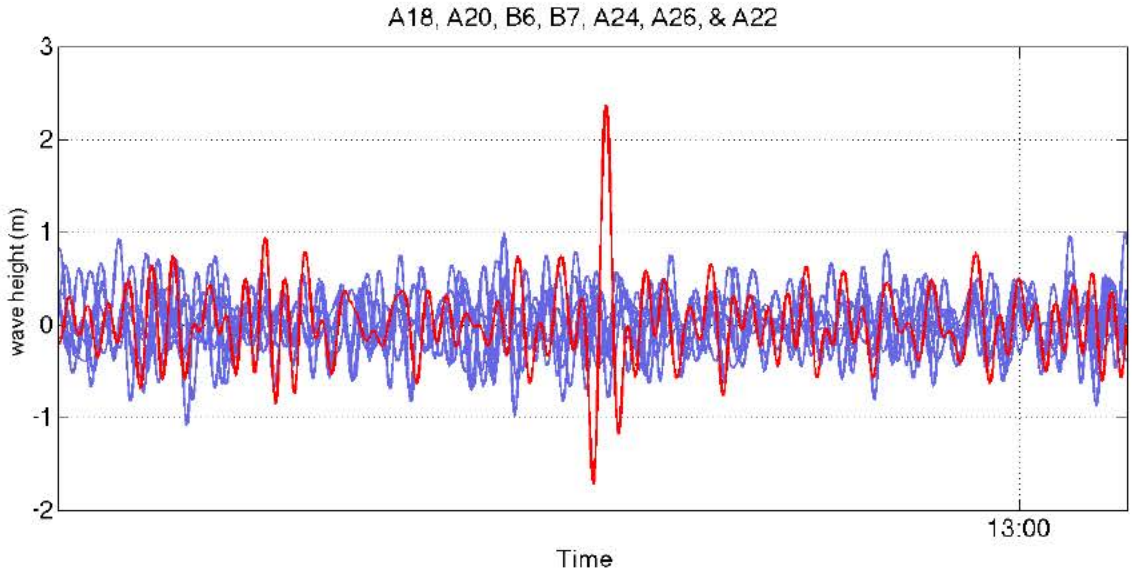

Figure 18. 5-minute time series for WRD A22 (in red) plotted against nearby buoys A18, A20, A24, A26, and B6 (in blue).

The area of interest was divided into ensembles by 2-minute longitude. Waves within each ensemble were placed into histograms for comparison with the Rayleigh probability density function, traced in red in each of the below histograms (Figure 19). Histograms for May 27 show general agreement with Rayleigh theory as seen by the area under the red curve. However, there are areas near the bar that show noticeable outliers from the density function and could either be a function of current focusing and refraction, or a by-product of having a relatively small wave sample as indicated by other areas in the histogram that do not strictly adhere to the curve. Regional wave ensemble 11, for example, experienced 7 waves that exceeded the threshold of $2.828H_{rms}$ out of the 2,244 waves in the histogram, accounting for 0.312% of the waves: more than 10 times what is predicted by Rayleigh theory.

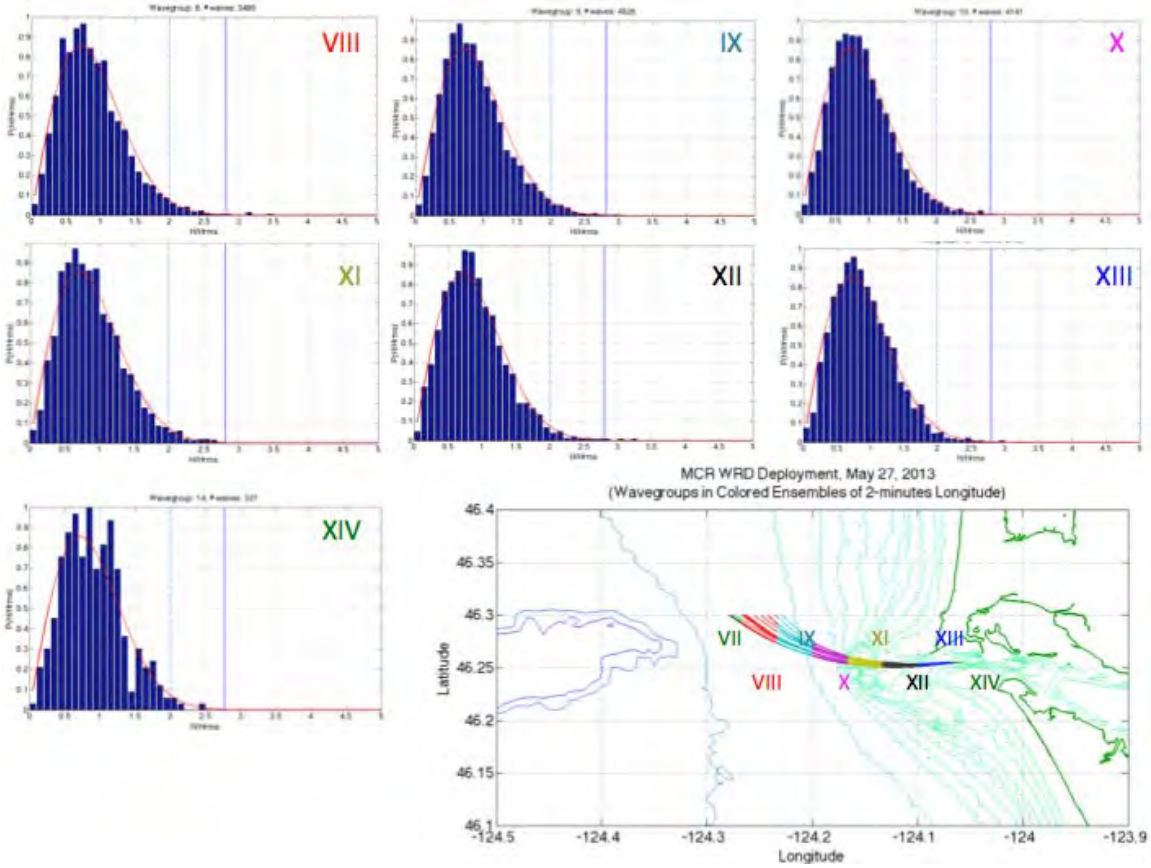

Figure 19. Each colored region shows the portion of the drifter tracks within a 2-minute longitude interval that constitutes one ensemble. Histograms are numbered according to their ensemble shown in chart. The theoretical Rayleigh pdf for a narrow band, Gaussian wave field (red curve) is superposed on each histogram.

B. MAY 29, 2013

On the second day of the field experiment, 44 WRDs collected more than 102,836 waves as they travelled over the bar and out to sea. Because the wave direction was predominantly from the southwest, once clear of the river outflow currents and ebb tide, the WRDs began to head north and back to the coast. The same northern latitude limit of 46.3°N was used to eliminate the areas that are not of interest, and to prevent the northern waves from contaminating sea state calculations when dividing waves into longitudinal regional ensembles. Of the more than 102,000 waves recorded, 37,705 waves were observed south of the defined latitude limit. Of these waves, 872 (2.31%%) were extreme waves, 33 (0.088%) of which were rogue waves. The offshore wave conditions were even

more benign on this day than on May 27, with an average wave height of 0.75 meters. Although the general sea state was gentler on May 29, the maximum-recorded wave, at 5.22 meters, exceeded the maximum-recorded wave on May 27.

Sea state was calculated for this day using the same method as before: for each wave by comparison with all surrounding waves within a 1-kilometer radius. Compared to the previous day, initial inspection would suggest the same general random distribution of extreme and rogue waves with a small concentration over the Bar (Figure 20). What is different about this day is the distinct lack of rogue waves as the waves head into shore just prior to the bar. While there are extreme waves observed throughout the area, the area just offshore from the Bar has only extreme waves and no rogue waves whatsoever. Once the waves transit onto the Bar, the formation of extreme and rogue waves is now present and concentrated in a small area (Figure 21). The second panel in Figure 20 shows the same gradual decrease in *Hrms* approaching the shore toward the Bar as noted in the previous day, but in contrast to the May 27 observations, May 29 shows a significant increase or amplification of wave height as they approach the Bar. This is largely due to the shift in wave direction from the south to a more eastward direction causing more refractive focusing (Pearman, 2014).

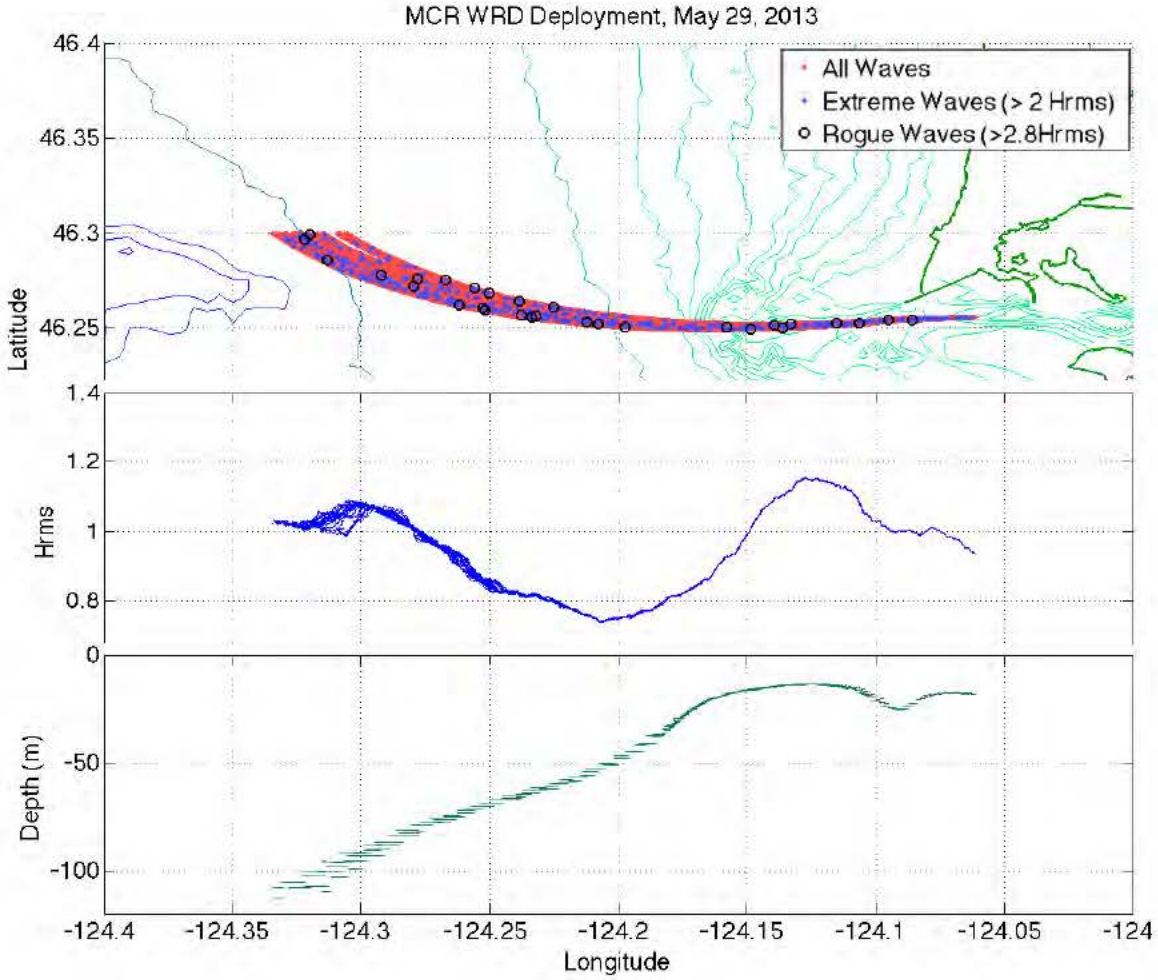

Figure 20. Top Panel: Wave heights of individual waves observed along the drifter tracks. From left to right, depth contours in meters are: 200, 150, 100, 50, 35, 30, 25, 22, 20, 18, 15, 12, 9. Middle panel: *Hrms* along each drifter track vs. longitude. Bottom panel: water depth along each drifter track vs. longitude.

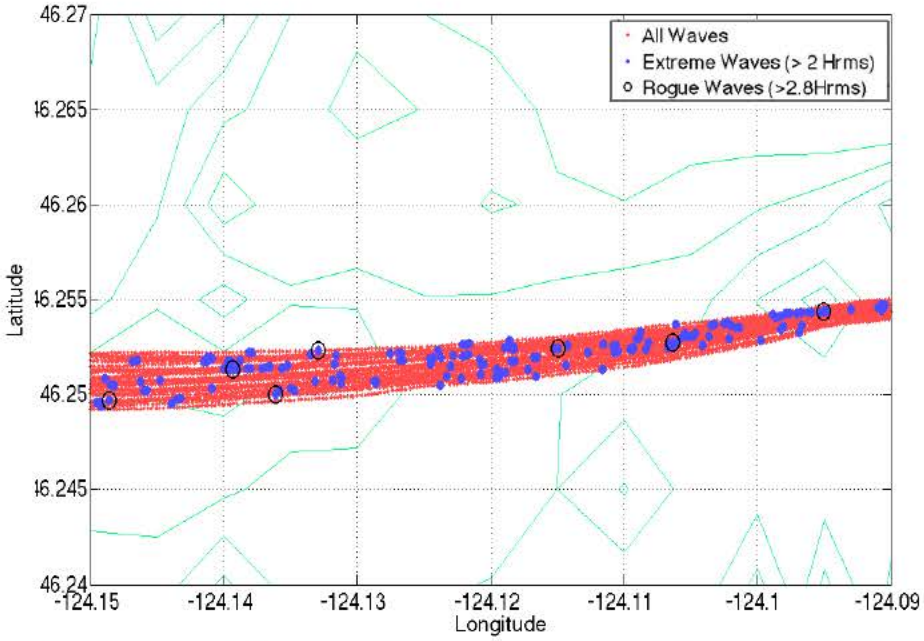

Figure 21. Blow up of the wave observations of Figure 20 for the Columbia River Bar area. Depth contours are from bottom left in meters: 30, 25, 22, 20, 18, 15, 9.

Investigating the time series for wave events for May 29 shows the same type of isolated wave that is both characteristic for what would normally by expected, and what was observed on May 27. The top panel in Figure 22 is an isolated 4-meter wave shown on a 5-minute time series for WRD A10. The bottom panel in Figure 22 is the time series for WRD A32 as it experienced the largest recorded wave of the day in the area of interest. This 5.071-meter wave was recorded in an area offshore of the Bar where the local sea state had an *Hrms* of 0.859 meters. This wave with more than twice the height of the rogue wave threshold clearly exemplifies the occurrence of an isolated rogue wave (Figure 22, bottom panel and the histogram shown in Fig. 23)!

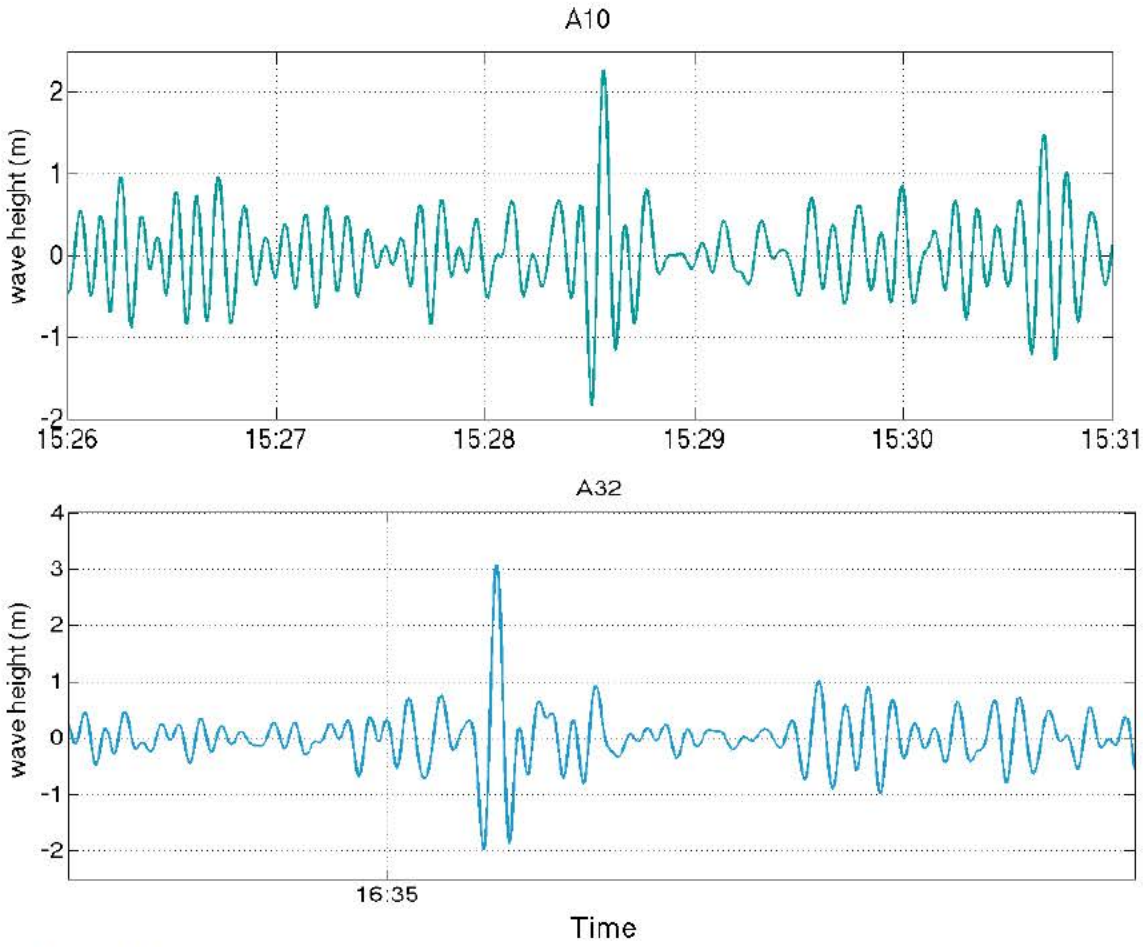

Figure 22. Both panels: 5-minute time series showing extreme wave events on May 29, 2013. Top panel: drifter A10 while transiting over the Bar. Bottom panel: 5.071-meter wave offshore from the Bar.

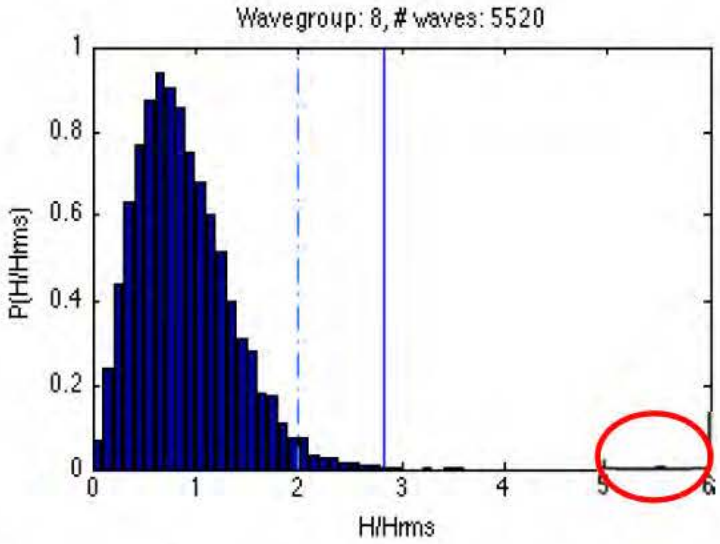

Figure 23. Histogram of regional ensemble #8 containing the largest wave in the area for the day (5.071m), circled in red.

When dividing the waves from May 29 into 2-minute longitude regional ensembles like on May 27 and concentrating in the areas closest to the Bar, again the occurrence of extreme and rogue waves generally followed the prediction from Rayleigh probability theory (Figure 24). Again, the exception was the area over the Bar. Although the waves on this day did not deviate as drastically as on the previous day, there was still an occurrence of rogue waves at a rate of ~3 times predicted by Rayleigh theory in regional ensemble #11 over the Bar.

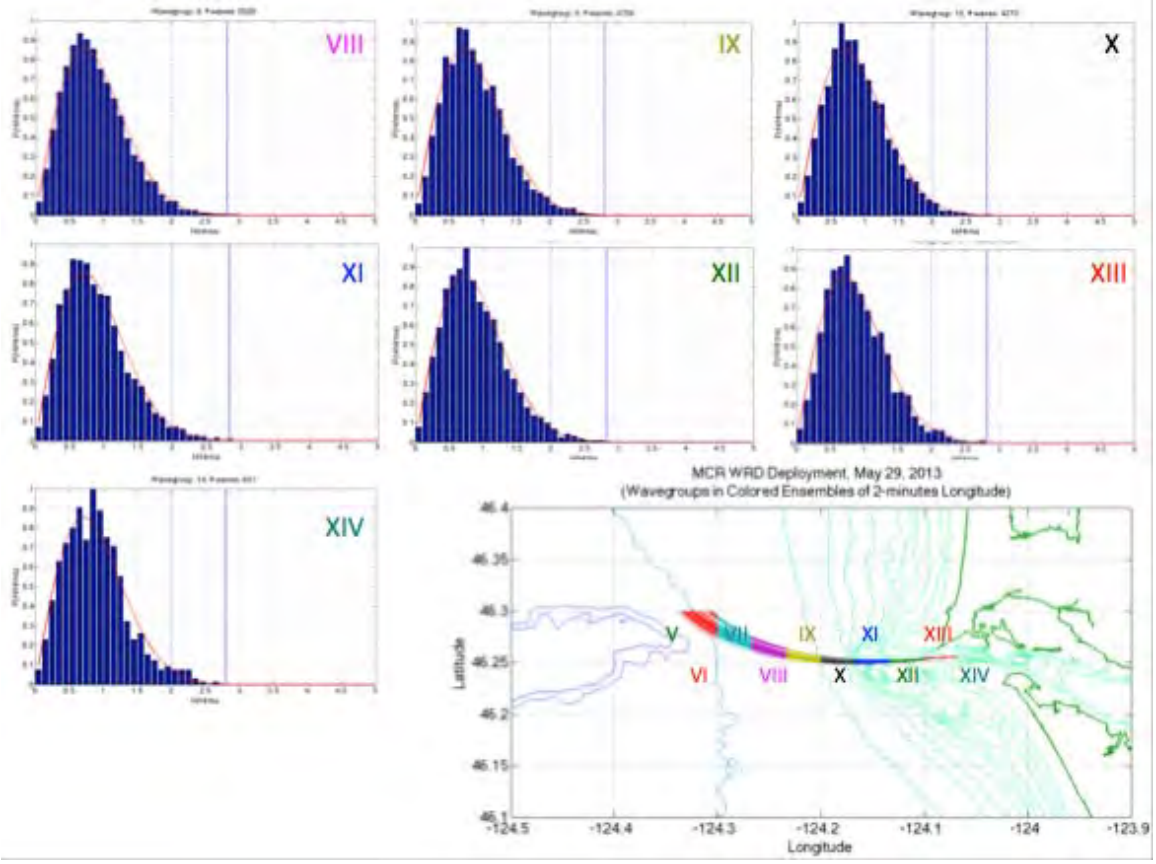

Figure 24. Each colored region shows the portion of the drifter tracks within a 2-minute longitude interval that constitutes one ensemble. Histograms are numbered according to their ensemble shown in chart. The theoretical Rayleigh pdf for a narrow band, Gaussian wave field (red curve) is superposed on each histogram.

C. JUNE 8, 2013

On June 8, 30 WRDs were deployed and drifted westward, well clear of the Bar, and continued west into the predominant waves from the west. The drifters maintained a westward course throughout the collection process and therefore there was no need to establish a northern latitude limit; 59,532 waves were collected. Of the waves recorded, 1,164 waves (1.955%) were extreme waves, 43 (0.072%) of which were rogue waves. There was a lower rate of rogue waves on this day than on the other 2 days, however the overall wave conditions were much higher. By far, this was the roughest day of the 3, with a mean wave height for the area of 1.38 meters: almost twice higher than either of the other two days. The maximum wave height for this day was 6.48 meters!

When looking at the top panel of Figure 25, there is the same general random distribution of extreme waves throughout the area. Important to note is the same lack of extreme waves approaching the Bar from offshore followed by a rapid increase and concentration of extreme waves on the Bar. Also of note in the middle panel is the same gradual decrease in *Hrms* as the waves approach the Bar where there is the rapid amplification of wave height as the waves transit onto the Bar. This large amplification of waves is consistent with what should be expected from refractive focusing from the Bar's topography (Pearman 2014).

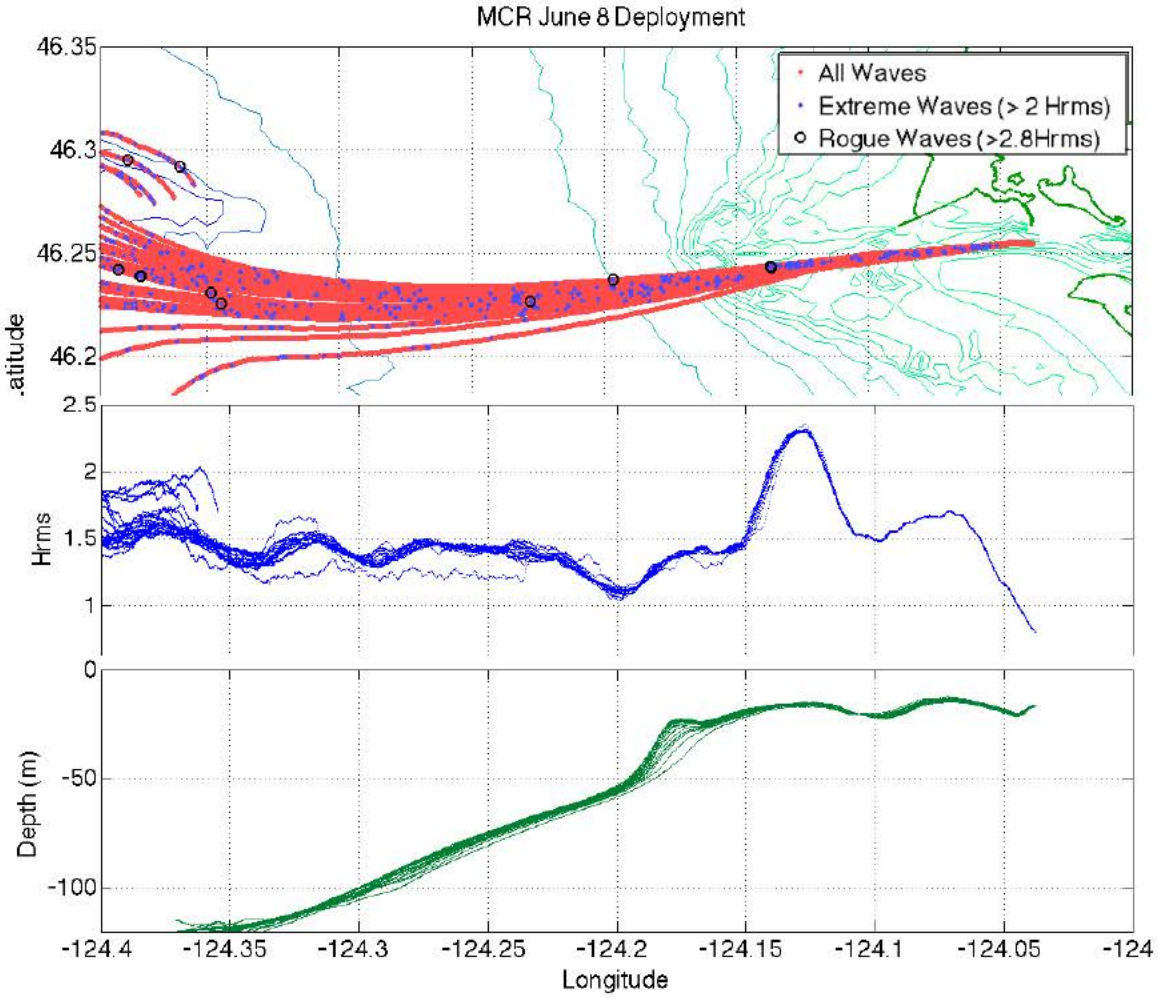

Figure 25. Top Panel: Wave heights of individual waves observed along the drifter tracks. From left to right, depth contours in meters are: 200, 150, 100, 50, 35, 30, 25, 22, 20, 18, 15, 12, 9. Middle panel: *Hrms* along each drifter track vs. longitude. Bottom panel: water depth along each drifter track vs. longitude.

When looking closer at the drifter tracks and extreme waves over the Bar (Figure 26), it should be noted that the southern drift tracks experienced no extreme waves whatsoever. While all the waves in this area are large due to the amplification of *Hrms* over the bar due to refractive focusing, none of the southern drifters experienced the extreme and rogue wave occurrences that the northern drifters experienced. The contours in the topography indicate that the northern drifters travelled closer to an area of increased shoaling whereas the southern drifters may not have been subjected to the same focusing caused by the topography because of the increased distance from it: the southern drifters also pass over an area of deeper topography.

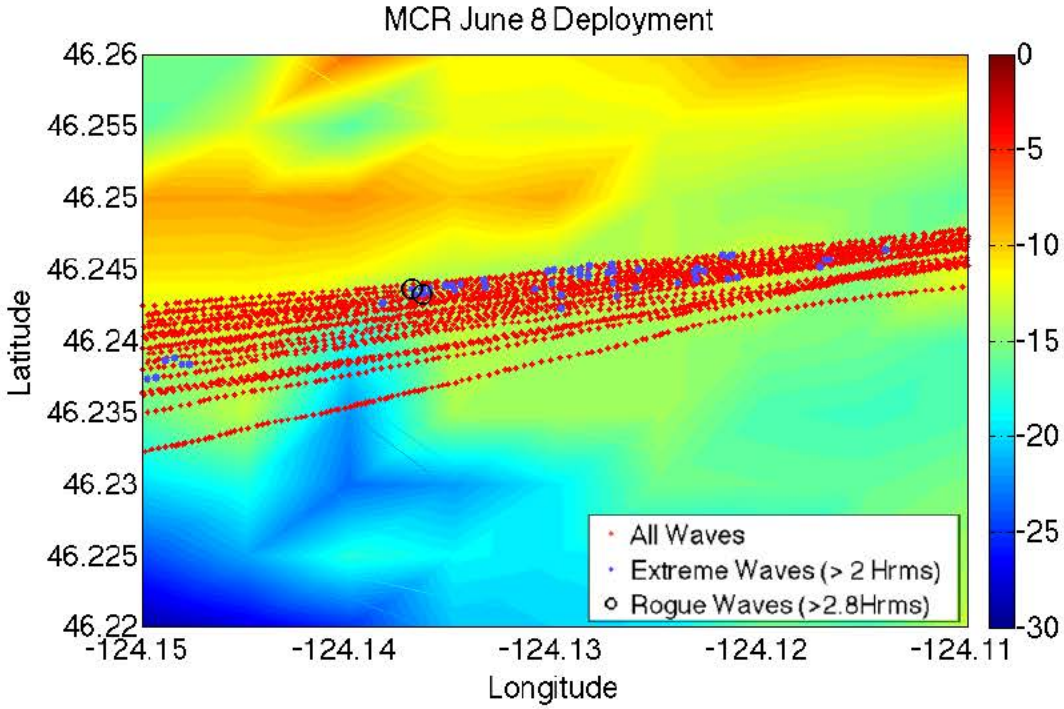

Figure 26. Blow up of the wave observations of Figure 25 for the Columbia River Bar area, showing wave events. Depth contours are from bottom left in meters: 30, 25, 22, 20, 18, 15, 9, and enhanced with color.

Investigating the time series for wave events over the Bar on June 8 shows the rapid amplification of wave height indicated by the increased average wave height. Figure 27 shows the northern drifters A16 and A17 during a 30-minute period travelling towards, over, and past the bar. The transit over the Bar is marked with 1–2.5 meter wave

heights followed by a 5–8 minute period of intense height amplification of waves routinely reaching in excess of 4 meters in rapid succession.

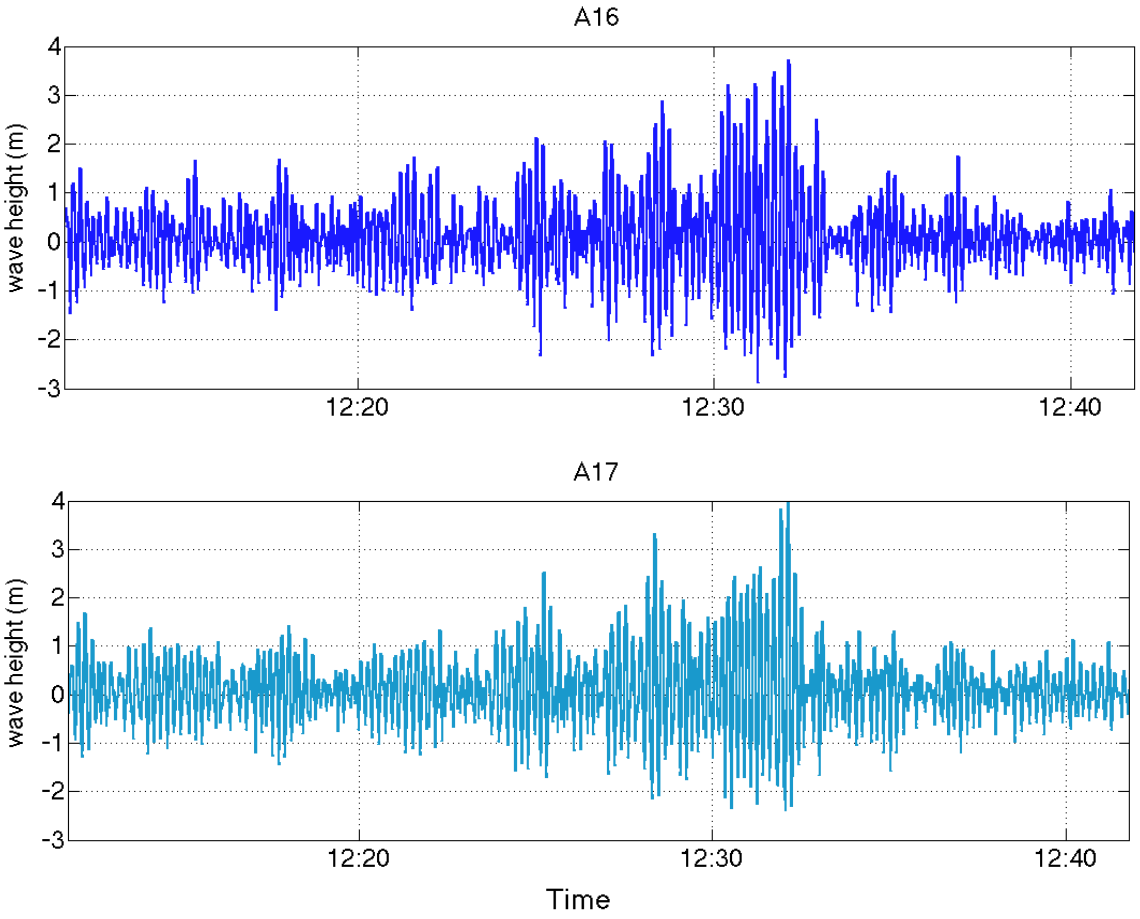

Figure 27. Both panels: 30-minute time series showing wave amplification over the Bar.

When comparing time series of the northern most drifter (A23) and the southern most drifter (B1) in Figure 28, drifter B1 experiences what could be considered a "normal" time series segment while virtually every wave during the 5-minute transit that drifter A23 experiences would be considered extreme in comparison to anything recorded by B1. However, because all the waves from all the drifters in the northern tracks were so high, most of them were not considered extreme; even less were considered rogue. The drifters in Figure 28 were only 600–800 meters apart during the indicated portion of their transit.

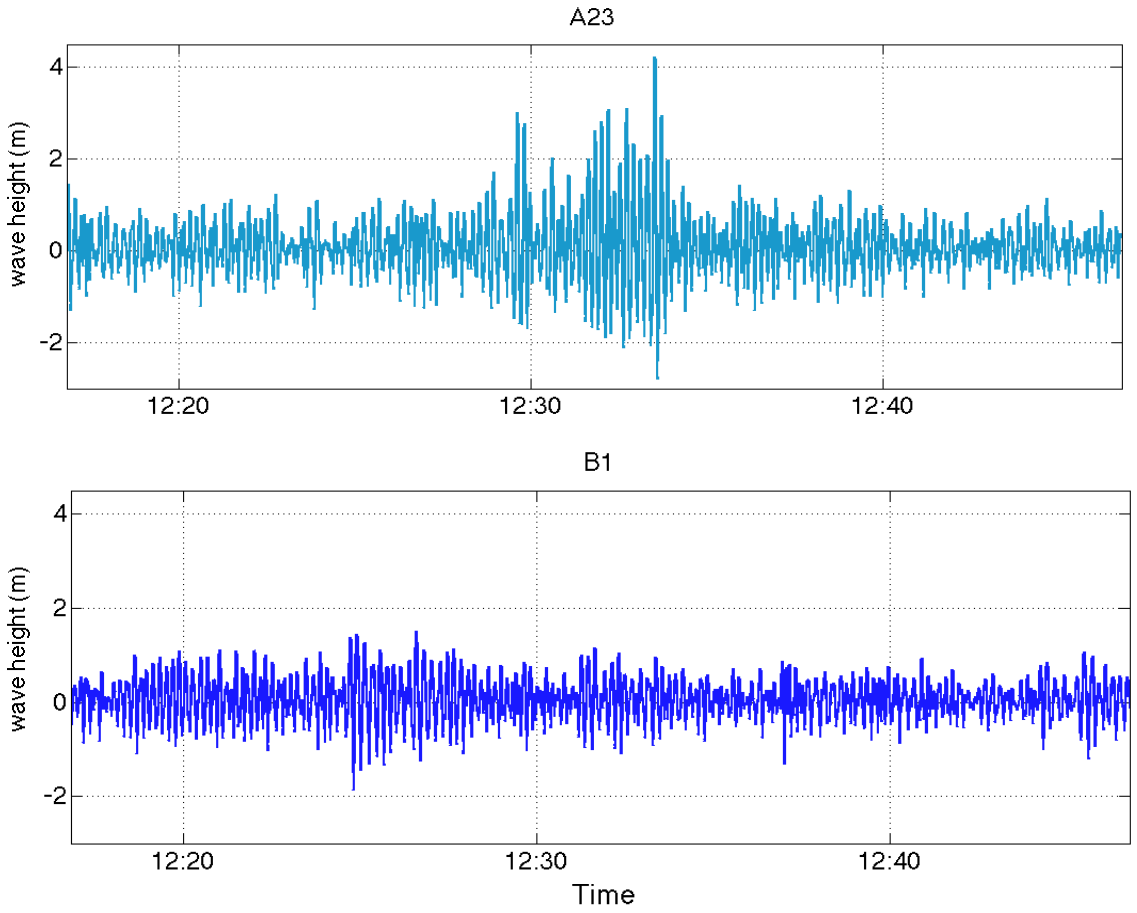

Figure 28. Histogram of regional ensemble #8 containing the largest wave in the area for the day (5.071m), circled in red.

The characteristic of extreme wave events experienced on June 8 is vastly different over the Bar than the isolated events experienced on the same day away from the Bar and on different days experienced even on the Bar.

The histograms shown for June 8th (Figure 29) were similar to the other days when considering the areas outside of the Bar where the histograms generally agreed with Rayleigh theory. However, on the Bar, more outliers were observed on June 8. Regional ensemble #11 had 11-recorded waves exceeding the 2.828*Hrms* threshold for rogue wave classification: for this day and in this area, a height of 3.237 meters! With the highest waves exceeding 4*Hrms*, the occurrence of rogue waves in this ensemble was 17 times more than what was expected from Rayleigh probability theory!

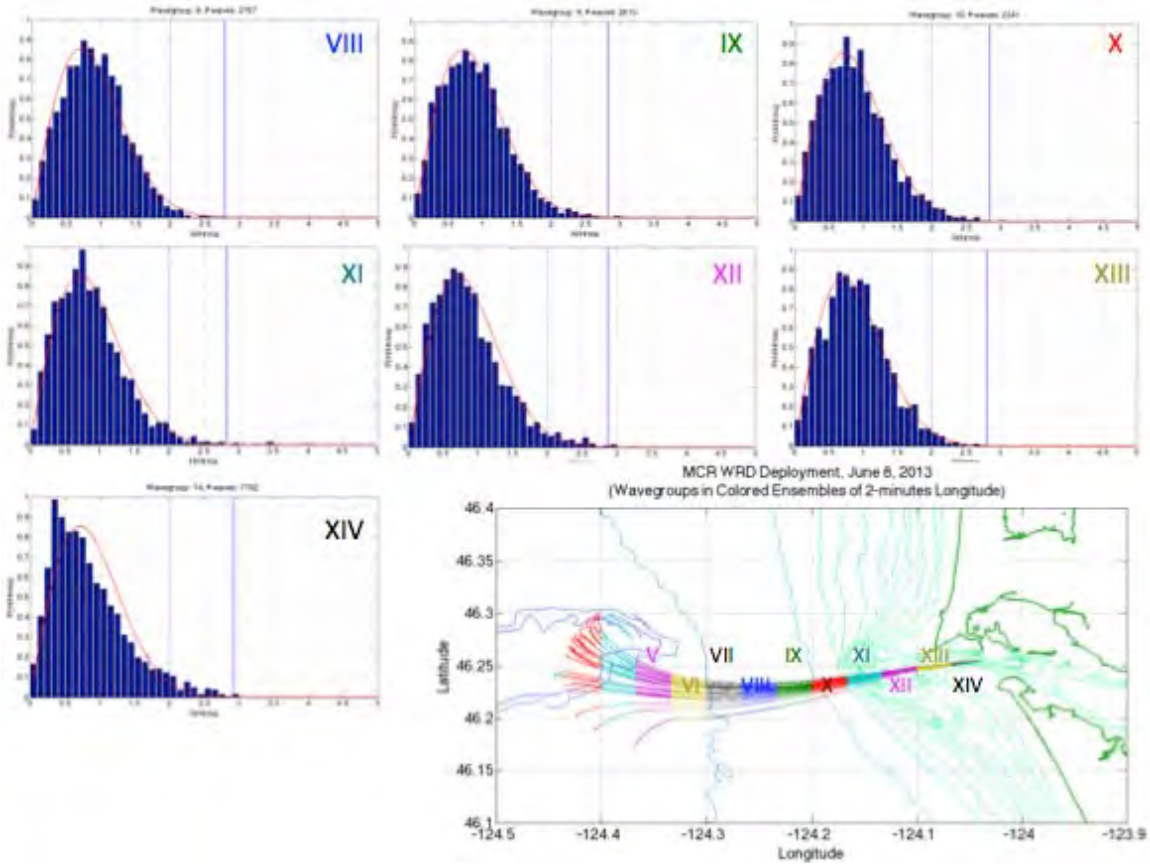

Figure 29. Each colored region shows the portion of the drifter tracks within a 2-minute longitude interval that constitutes one ensemble. Histograms are numbered according to their ensemble shown in chart. The theoretical Rayleigh pdf for a narrow band, Gaussian wave field (red curve) is superposed on each histogram.

THIS PAGE INTENTIONALLY LEFT BLANK

V. CONCLUSIONS AND FUTURE RESEARCH

This thesis examines the characteristics of extreme and rogue waves as observed by mass deployments of wave resolving drifters in the Mouth of the Columbia River during three different data collection days during the Spring season, when river run-off coupled with ebb tides produces strong currents in the river mouth. Very few measurements had previously been taken in this extremely dynamic environment on and in the vicinity of the Columbia River Bar. Through the examination of time series for wave events, the calculations of local sea states, and the comparison of statistical regional ensemble histograms for each day, the occurrence of extreme waves is characterized within the Mouth of the Columbia River.

Consistent with previous research by Janssen and Herbers (2009), the Columbia River Bar area of the MCR creates strong, refractive focusing in wave conditions that are already amplified by the shallower bottom topography, creating conditions conducive to rogue wave development. The Bar is an area with routinely amplified waves averaging over one meter in height. Given strong river outflow current from the east colliding with predominant wave trains from the west, wave heights in this area will be rapidly amplified through refractive focusing of currents, achieving heights in excess of 6 meters, more than 5 times the ambient sea state.

Both isolated rogue waves and trains of large waves were observed on the MCR Bar. On a relatively calm day with waves from the South or South-southwest, amplification over the Bar was less significant and the occurrence of extreme and rogue waves followed the more conventional expectation of single, isolated waves. On June 8, with the waves travelling from the West, the occurrence of extreme and rogue waves most often occurred in trains of very large waves, some of which no longer met the criteria for being considered extreme waves due to the close proximity of other very large waves.

Because the sea state in the MCR Bar area varies on scales less than a few km, the unintentional inclusion of waves from different regimes may result in errors when

calculating sea states. Histogram analysis makes the assumption that all waves within a particular wave ensemble experience the same sea state. While this assumption is easily satisfied for a fixed sensor over a relatively short period of time, when using WRDs, sea state consistency becomes difficult in a bathymetrically dynamic region that experiences localized sea state variation due to refractive focusing caused by the underwater topography and opposing currents. Because of the challenges involved in a spatially dynamic sea state area and the short time frame WRDs may spend in particular wave regime, a delicate balance must be found between wave regime and wave population. If the wave ensemble area chosen is too large, several wave regimes may be included in the histogram, which contaminates the statistics. Although the sea state may be consistent throughout a wave ensemble histogram, if the wave ensemble area is not large enough, the number of observed waves may be insufficient to discern meaningful results from the histogram.

When attempting to strike the delicate balance of sea state variations versus wave population, 5-minute longitudinal regional ensembles were found to cover too broad an area: the significance of the large waves was averaged out because of the large number of waves covering more than one wave regime. As a result, all waves within this broad ensemble fit well within the Rayleigh probability distribution function.

Having too narrow an ensemble caused difficulties of their own as well: generally, too narrow an area caused very choppy results that left more to subjective intuition than scientific objectivity. The 2-minute longitude regional ensembles used in this thesis appeared to provide a reasonable compromise, although attention had to be paid to wave ensemble placement as the refraction induced sea state variations were abrupt over the Bar.

Generally, there are more rogue waves than predicted by the Rayleigh pdf over the Bar. However, for the reasons stated above, traditional sea state considerations do not adequately capture the Bar's wave significance, especially when considering Safety of Navigation. Although on June 8th, less rogue waves were common on the Bar, the height of these waves compared to other days in the same region, or waves during the same day in an area 600 meters away, were extremely large and frequent.

With the advancement in technology reducing the cost of these wave resolving drifter buoys, there is an increased opportunity to conduct mass drifter deployments for the study of rogue waves in the nearshore and river mouth environments. Where the dynamic environment of massive, tossing waves and strong currents is utterly inhospitable to the installation and maintenance of fixed sensors, the deployment of WRDs is ideal in collecting data under these demanding conditions. Further study in the MCR during the harsh winter months, as well as more deployment days during the springtime snowmelt season would provide more invaluable data in the Mouth of Columbia River. In both instances using 30–50 drifters to collect data in the area of intense refractive focusing over the Bar, where the drifters only spend 5–10 minutes of transit, would benefit the most from the large volume of drifters deployed over several days or weeks. More research into why the vast differences in waves experienced on June 8th over the Bar, often within a few short wavelengths of one another, would provide more insight into the dynamics in the area.

Understanding the processes that influence extreme and rogue wave generation in the coastal, river mouth, and shoaling environment will have a positive impact on safety of navigation near shore, but may also contribute to the overall understanding of rogue wave principles in this relatively new area of scientific research.

THIS PAGE INTENTIONALLY LEFT BLANK

APPENDIX A. SCRIPP'S WAVERIDER BUOY DATA

Station 46243 - Clatsop Spit, OR

#YY	MM	DD	hh	mm	WVHT	DPD	APD	MWD	WTMP
#yr	mo	dy	hr	mn	m	sec	sec	deg	degC
2013	5	27	12	10	1.62	5.88	5.16	206	13.2
2013	5	27	12	40	1.63	6.67	4.97	214	13.2
2013	5	27	13	10	1.8	6.25	5.19	197	13.2
2013	5	27	13	40	1.82	6.67	5.23	202	13.1
2013	5	27	14	10	1.88	6.67	5.48	203	13.1
2013	5	27	14	40	2.08	6.25	5.67	202	13.1
2013	5	27	15	10	2.28	7.14	5.97	203	13
2013	5	27	15	40	2.58	7.69	6.02	214	13
2013	5	27	16	10	2.71	7.69	6.2	211	13
2013	5	29	14	40	1.32	9.09	7.83	248	13
2013	5	29	15	10	1.31	9.09	7.79	241	13
2013	5	29	15	40	1.48	8.33	7.65	237	13.1
2013	5	29	16	10	1.44	9.09	7.61	237	13.1
2013	5	29	16	40	1.54	7.69	7.47	207	13.4
2013	5	29	17	10	1.82	8.33	7.36	216	13.5
2013	5	29	17	40	1.78	7.69	7.13	213	13.6
2013	5	29	18	10	2.11	7.69	7.4	202	13.9
2013	6	8	11	10	2.06	18.18	10.43	231	13.3
2013	6	8	11	40	2.07	15.38	9.83	261	12.5
2013	6	8	12	10	2.03	16.67	10.25	231	11.7
2013	6	8	12	40	2.3	16.67	11.31	247	12.3
2013	6	8	13	10	2.22	15.38	11.1	252	12.3
2013	6	8	13	40	2.64	15.38	11.87	252	12.3
2013	6	8	14	10	2.49	15.38	11.63	256	13.2
2013	6	8	14	40	2.35	16.67	11.27	231	13.7
2013	6	8	15	10	2.27	13.33	10.96	258	13.9

THIS PAGE INTENTIONALLY LEFT BLANK

APPENDIX B. SCRIPP'S WAVERIDER BUOY DATA

Station 46248 - Astoria Canyon, OR

#YY	MM	DD	hh	mm	WVHT	DPD	APD	MWD	WTMP
#yr	mo	dy	hr	mn	m	sec	sec	degT	degC
2013	5	27	12	6	2.62	6.67	5.66	174	11.8
2013	5	27	12	36	2.81	6.67	5.76	171	11.8
2013	5	27	13	6	3.31	7.14	6.12	183	11.8
2013	5	27	13	36	3.06	7.69	6.1	183	11.7
2013	5	27	14	6	3.32	7.69	6.27	190	11.6
2013	5	27	14	36	3.48	7.14	6.35	185	11.5
2013	5	27	15	6	3.51	7.69	6.69	185	11.6
2013	5	27	15	36	3.31	8.33	6.6	202	11.4
2013	5	27	16	6	3.55	8.33	6.88	189	11.3
2013	5	29	14	36	1.59	8.33	6.29	249	11.7
2013	5	29	15	6	1.76	8.33	6.59	256	11.8
2013	5	29	15	36	2	9.09	6.89	252	11.8
2013	5	29	16	6	2.09	7.69	6.97	206	11.9
2013	5	29	16	36	2.08	7.69	6.97	206	11.9
2013	5	29	17	6	2.26	7.14	7.04	203	11.9
2013	5	29	17	36	2.05	7.69	6.93	193	12
2013	5	29	18	6	2.14	8.33	6.8	206	12
2013	6	8	11	6	2.91	15.38	10.13	280	14.1
2013	6	8	11	36	2.85	16.67	10.85	265	14.1
2013	6	8	12	6	2.73	14.29	10.28	276	14.1
2013	6	8	12	36	2.68	15.38	10.52	287	14.1
2013	6	8	13	6	2.33	15.38	9.86	289	14.1
2013	6	8	13	36	2.43	14.29	10	279	14.1
2013	6	8	14	6	2.62	15.38	10.43	280	14
2013	6	8	14	36	2.44	15.38	10.34	275	14
2013	6	8	15	6	2.52	14.29	10.23	280	13.9

THIS PAGE INTENTIONALLY LEFT BLANK

APPENDIX C. NOAA STATION WATER LEVEL OBSERVATION NETWORK

Station ASTO3-9439040 - Astoria, OR

#YY	MM	DD	hh	mm	WDIR	WSPD	GST	PRES	ATMP	WTMP
#yr	mo	dy	hr	mn	degT	m/s	m/s	hPa	degC	degC
2013	5	27	12	0	313	2.1	4.3	1009.2	11.2	15.1
2013	5	27	12	6	268	1.5	5.5	1009	11.2	15.1
2013	5	27	12	12	341	2.6	5.2	1008.9	11.2	15.1
2013	5	27	12	18	332	2.8	5.1	1008.8	11.1	15.1
2013	5	27	12	24	231	1.5	4.8	1008.6	11.2	15.1
2013	5	27	12	30	276	2	4.1	1008.5	11.2	15.1
2013	5	27	12	36	337	3.4	5.2	1008.3	11.2	15.1
2013	5	27	12	42	246	1.9	4.3	1008.3	11.2	15.1
2013	5	27	12	48	238	1.9	4.4	1008.2	11.3	15.1
2013	5	27	12	54	162	1.4	4.1	1008.1	11.3	15.1
2013	5	27	13	0	177	1.6	2.8	1008	11.2	15.1
2013	5	27	13	6	139	2.1	3.6	1007.8	11.2	15.1
2013	5	27	13	12	154	1.9	3.8	1007.7	11	15.1
2013	5	27	13	18	94	1.7	3.2	1007.6	11.2	15.1
2013	5	27	13	24	133	2.3	5.2	1007.6	11.2	15.1
2013	5	27	13	30	269	1.4	2.5	1007.5	11.3	15.1
2013	5	27	13	36	146	2.5	4.4	1007.4	11.1	15.1
2013	5	27	13	42	145	3.1	5.6	1007.3	11.3	15.1
2013	5	27	13	48	193	1.6	4.9	1007.2	11.2	15.1
2013	5	27	13	54	158	3.4	5.7	1007.2	11.2	15.1
2013	5	27	14	0	155	2.5	5.4	1007	11.2	15.1
2013	5	27	14	6	173	1.8	4.3	1007.1	11.2	15.1
2013	5	27	14	12	120	1.3	2.5	1007	11.3	15
2013	5	27	14	18	162	3	5.2	1006.9	11.4	15.1
2013	5	27	14	24	141	1.9	4.9	1006.9	11.4	15.1
2013	5	27	14	30	170	2.5	4.7	1006.8	11.4	15
2013	5	27	14	36	166	2.8	4.8	1006.8	11.4	15
2013	5	27	14	42	152	2.9	5.8	1006.8	11.4	15.1
2013	5	27	14	48	194	1.3	4.8	1006.7	11.4	15.1
2013	5	27	14	54	160	3.5	4.9	1006.7	11.4	15.1
2013	5	27	15	0	239	1.1	4	1006.6	11.4	15.1

2013	5	27	15	6	144	1.9	3.3	1006.5	11.4	15.1
2013	5	27	15	12	192	1.5	4.1	1006.5	11.4	15.1
2013	5	27	15	18	142	2.4	5.6	1006.4	11.5	15.2
2013	5	27	15	24	162	2.9	4.6	1006.4	11.5	15.2
2013	5	27	15	30	153	2.6	5.3	1006.4	11.6	15.2
2013	5	27	15	36	133	0.9	2.9	1006.2	11.6	15.2
2013	5	27	15	42	185	0.7	1.7	1006.2	11.5	15.2
2013	5	27	15	48	135	1.3	3.3	1006.1	11.6	15.2
2013	5	27	15	54	104	0.2	2	1006	11.6	15.2
2013	5	27	16	0	111	0.7	1.7	1006	11.6	15.2
2013	5	27	16	6	68	1.1	2.3	1005.9	11.7	15.2
2013	5	27	16	12	348	0.9	3.5	1005.8	11.8	15.2
2013	5	29	14	42	342	2.5	3.4	1005.6	11.1	15.6
2013	5	29	14	48	320	2.3	3.3	1005.7	11.3	15.7
2013	5	29	14	54	319	2.2	3.4	1005.8	11.5	15.7
2013	5	29	15	0	315	1.9	2.8	1005.9	11.8	15.7
2013	5	29	15	6	298	1.2	2.5	1006.1	11.8	15.7
2013	5	29	15	12	15	0.2	1.4	1006.3	12	15.6
2013	5	29	15	18	334	0.8	2	1006.4	12	15.6
2013	5	29	15	24	307	0.9	2.4	1006.6	11.9	15.6
2013	5	29	15	30	290	1.2	2.9	1006.8	11.8	15.7
2013	5	29	15	36	172	0.6	2.4	1006.9	11.9	15.7
2013	5	29	15	42	257	1.7	4.4	1007.1	11.8	15.6
2013	5	29	15	48	230	1.5	3.7	1007.2	11.7	15.6
2013	5	29	15	54	252	2.4	4.7	1007.3	11.7	15.7
2013	5	29	16	0	259	2.3	5.5	1007.5	11.8	15.7
2013	5	29	16	6	244	1.4	4.6	1007.6	11.9	15.7
2013	5	29	16	12	245	1	4	1007.8	12.1	15.7
2013	5	29	16	18	303	0.8	2.7	1007.8	12.1	15.7
2013	5	29	16	24	249	1.7	3.9	1007.9	12.1	15.7
2013	5	29	16	30	248	2.7	4.8	1008	12.1	15.7
2013	5	29	16	36	259	1.4	3.8	1008.1	12.3	15.7
2013	5	29	16	42	269	2	4.8	1008.3	12.3	15.8
2013	5	29	16	48	260	1.4	4.6	1008.4	12.4	15.8
2013	5	29	16	54	272	1.3	4.6	1008.5	12.4	15.8
2013	5	29	17	0	263	2.2	4.3	1008.6	12.5	15.8
2013	5	29	17	6	211	1.1	4.5	1008.8	12.7	15.8
2013	5	29	17	12	333	0.7	3.1	1008.9	12.8	15.8
2013	5	29	17	18	259	2.5	5.7	1009	12.7	15.8

2013	5	29	17	24	267	1.4	4.9	1009.2	12.8	15.9
2013	5	29	17	30	256	4.3	8	1009.4	12.6	15.9
2013	5	29	17	36	254	4.9	8.2	1009.5	12.4	15.9
2013	5	29	17	42	253	5.5	9	1009.6	12.4	15.9
2013	5	29	17	48	256	4.9	9.2	1009.7	12.4	15.9
2013	5	29	17	54	251	4.9	8.6	1009.8	12.5	15.9
2013	5	29	18	0	254	4.6	8	1009.9	12.5	15.9
2013	5	29	18	6	246	4	7.4	1010.1	12.6	15.9
2013	5	29	18	12	250	4.6	7.6	1010.2	12.6	15.9
2013	6	8	11	6	346	2.9	4	1022.6	12.5	17.5
2013	6	8	11	12	3	3	3.8	1022.6	12.4	17.5
2013	6	8	11	18	357	3.4	4.5	1022.7	12.3	17.5
2013	6	8	11	24	342	2.6	4.9	1022.7	12.4	17.5
2013	6	8	11	30	354	3	4	1022.7	12.3	17.5
2013	6	8	11	36	343	3	3.9	1022.8	12.3	17.5
2013	6	8	11	42	354	2.6	3.6	1022.7	12.4	17.5
2013	6	8	11	48	347	1.6	3.2	1022.6	12.2	17.5
2013	6	8	11	54	8	1.1	2.3	1022.6	12.2	17.5
2013	6	8	12	0	18	0.8	1.7	1022.7	12	17.6
2013	6	8	12	6	9	2.2	3.3	1022.7	12.2	17.5
2013	6	8	12	12	22	2.9	3.6	1022.7	12	17.5
2013	6	8	12	18	48	0.5	2.7	1022.8	11.8	17.5
2013	6	8	12	24	23	0.4	1.6	1022.9	11.8	17.6
2013	6	8	12	30	64	0.9	1.9	1022.8	11.8	17.6
2013	6	8	12	36	48	1.2	1.6	1022.7	11.7	17.6
2013	6	8	12	42	72	0.6	1.2	1022.8	11.6	17.6
2013	6	8	12	48	51	0.8	1.4	1022.7	11.5	17.6
2013	6	8	12	54	49	1.3	1.5	1022.8	11.6	17.6
2013	6	8	13	0	6	1.2	2	1022.9	11.7	17.6
2013	6	8	13	6	9	1.7	2.3	1023	11.7	17.6
2013	6	8	13	12	51	0.7	1.4	1022.8	11.8	17.6
2013	6	8	13	18	77	0.8	1.7	1022.8	11.7	17.6
2013	6	8	13	24	81	0.4	1.5	1022.7	11.8	17.6
2013	6	8	13	30	65	0.7	1.9	1022.7	11.8	17.6
2013	6	8	13	36	17	0.8	1.3	1022.8	11.9	17.6
2013	6	8	13	42	25	0.9	1.6	1022.8	11.9	17.6
2013	6	8	13	48	39	0.6	0.9	1022.6	11.8	17.5
2013	6	8	13	54	47	0.4	0.8	1022.6	11.8	17.5
2013	6	8	14	0	72	0.1	1.2	1022.5	11.8	17.4

2013	6	8	14	6	83	0.6	0.8	1022.6	11.9	17.4
2013	6	8	14	12	72	0.1	0.6	1022.8	11.9	17.4
2013	6	8	14	18	344	1.2	2.4	1022.9	12.1	17.4
2013	6	8	14	24	313	1.4	2.9	1022.7	12.2	17.4
2013	6	8	14	30	340	1.2	2.7	1022.9	12.3	17.4
2013	6	8	14	36	348	1.5	2.3	1022.9	12.3	17.4
2013	6	8	14	42	4	1.1	2	1022.8	12.4	17.4
2013	6	8	14	48	41	0.5	1.6	1022.8	12.5	17.4
2013	6	8	14	54	7	1	1.4	1022.9	12.4	17.3
2013	6	8	15	0	10	0.7	1.7	1022.9	12.5	17.4
2013	6	8	15	6	30	1.3	1.8	1022.8	12.3	17.5
2013	6	8	15	12	12	1.4	2.2	1022.8	12.3	17.5

LIST OF REFERENCES

Booij, N., R. C. Ris, and L. H. Holthuijsen, 1999: A third-generation wave model for coastal regions, Part 1, Model description and validation. *J. Geoph. Research*, C4, **104,** 7649-7666.

British Broadcasting Corporation, cited 2014: Horizon "Freak Wave." [available online at http://www.bbc.co.uk/science/horizon/2002/freakwave.shtml.]

Busch, H., See Funk Netz, cited 2014: Der Untergang der München /DEAT. [available online at http://www.seefunknets.de/deat.htm.]

Clauss G. F., M. Klein, 2009: The New Year Wave: Spatial Evolution of an Extreme Sea State *J. Offshore Mech. Arct. Eng.* **131**, 041001 (9 pages); doi:10.1115/1.3160533

Dawson, T.H., 1997: Group Structure in Random Seas. *J. Atmos. Oceanic Technol.,* **14**, 741-747. doi: 10.1175/1520-0426(1997)014<0741:GSIRS>2.0.CO;2

Dysthe, K.B., 1996: A modified nonlinear Schrodinger equation for broader bandwidth gravity waves on deep water. *Wave Motion,* **24,** 281-289.

Dysthe, K.B., Krogstad, H.E., Socquet-Juglard, H., and Turlsen, K., cited 2014. Freak Waves, Rogue Waves, Extreme Waves and Ocean Wave Climate. [available online at http://folk.uio.no/karstent/waves/index_en.html.

Elias, E. P. L., G. Gelfenbaum, and A. J. Van der Westhuysen, 2012: Validation of a coupled wave-flow model in a high-energy setting: The mouth of the Columbia River. *J. Geophys. Res.,* **117,** C09011, doi: 10.1029/2012JC008105.

Forristall, G. Z., 2000: Wave crest distributions: observations and second-order theory. *J. Phys. Oceanogr.,* **30**, 8, 1931–1943.

Haver, S., and O. J. Anderson, 2000. "Freak Waves: Rare Realization of a Typical Population or Typical Realization of a Rare Population?" *Proceedings of the Tenth International Offshore and Polar Engineering Conference*, ISOPE, Seattle, pp. 123–130.

Herbers, T. H. C., and Coauthors, 2012: Observing ocean surface waves with GPS-tracked buoys. *J. Atmos. Oceanic Technol.*, **29,** 944–959.

Janssen, Tim T. & T. H. C. Herbers, 2009: Nonlinear Wave Statistics in a Focal Zone. *J. Phys. Ocean.*, **39**, 1948–1964.

Janssen, T. T., and T. H. C. Herbers, 2011: *Wave-Current Interaction in Coastal Inlets and River Mouths*, Office of Naval Research.

Map Bureau, Columbia River Maritime Museum, cited 2014. Shipwrecks at the Mouth of the Columbia (picture). [available online at http://www.mapbureau.com:8080/launch/shipwrecks/.]

McIntyre, S. A., 2013: Wave and Current Observations in a Tidal Inlet Using GPS Drifter Buoys. Master's thesis, Graduate School of Engineering and Applied Sciences, Naval Postgraduate School. [available online at http://hdl.handle.net/10945/32869].

Mori, N. P., and A. E. M. Janssen, 2006: On Kurtosis and Occurrence Probability of Freak Waves. *J. Phys. Oceanogr.*, **36**, 1471–1483. doi: 10.1175/JPO2922.1

Naval History and Heritage Command, cited 2014: Wreck of the Memphis (photo). [available at http://www.history.navy.mil.]

NOAA – National Oceanic and Atmospheric Administration, cited 2014. National Data Buoy Center. Center for Excellence in Marine Technology. [available online at http://www.ndbc.noaa.gov.]

COMET – The University Corporation for Atmospheric Research, cited 2014.

Norton, J.D., cited 2014. The Quantum Theory of Waves and Particles. [available online at http://www.pitt.edu/~jdnorton/teaching/HPS_0410/chapters/quantum_theory_waves/index.html.]

Pararas-Carayannis, G., 2007: The Loss of the USS Memphis on 29 August 1916 – Was a Tsunami Responsible? Analysis of a Naval Disaster.

Pearman, D. W., 2014: Wave Evolution in River Mouths and Tidal Inlets. Naval Postgraduate School, 105 pp.

Portell, J. R., 2013: Calibration and Validation of Inertial Measurement Unit for Wave Resolving Drifters. Graduate School of Engineering and Applied Sciences, Naval Postgraduate School, 83 pp.

Rosenthal, W., and S. Lehner, 2008: Rogue Waves: Results of the MaxWave Project, *J. Offshore Mech. Arct. Eng.* **130**, 021006 (8 pages); doi:10.1115/1.2918126

Smith, C. B., 2006: *Extreme Waves.* National Academies Press, 320 pp.

Stansell, P., 2004: Distributions of freak wave heights measured in the North Sea. *Applied Ocean Research,* **26,** 35–48.

Taylor, P. H., cited 2014. The Shape of the Draupner Wave of 1st January 1995. [available online at http://www.icms.org.uk/archive/meetings/2005/roguewaves/presentations/Taylor.pdf.]

Thornton, E. B. and R. T. Guza, 1983: Transformation of Wave Height Distribution, *J. Geoph. Research.* **88**, 5925–5938.

University Corporation for Atmospheric Research, COMET, cited 2014. Wave Life Cycle II: Propagation & Dispersion. [available online at http://www.meted.ucar.edu/marine/mod3_wlc_prodis/index.htm.]

White, B.S., and B. Fornberg, 1998: On the Chance of Freak Waves at Sea. *J. Fluid Mech.* **355**, 113–138.

Wikipedia, cited 2014. Columbia Bar (picture). [available online at http://en.wikipedia.org/wiki/Columbia_Bar#mediaviewer/File:Columbia_River_Bar-en.svg.]

THIS PAGE INTENTIONALLY LEFT BLANK

INITIAL DISTRIBUTION LIST

1. Defense Technical Information Center
   Ft. Belvoir, Virginia

2. Dudley Knox Library
   Naval Postgraduate School
   Monterey, California